# 1
# A Brief Overview of the Mechanisms Involved in Electrospray Mass Spectrometry

*Paul Kebarle and Udo H. Verkerk*

## 1.1
## Introduction

### 1.1.1
### Origins of Electrospray Mass Spectrometry

Electrospray Ionization (ESI) is a method by which solutes present in a solution can be transferred into the gas phase as ions. The gas-phase ions can then be detected by mass spectrometric means (ESI-MS). Remarkably, ESI can handle a vast variety of analytes from small inorganic or organic species to polymers, nucleic acids, and proteins of very high molecular mass. The analytes present in the solution may be positive or negative ions, or compounds that are not ionized in the solution that is sprayed. In that case the analyte is charged by association with one or more of the ions present in the solution. This charging process is part of the electrospray mechanism. ESI-MS is an excellent method for detection of analytes generated by high-pressure liquid chromatography or capillary electrophoresis. As a result, scientists in biochemical, biomedical, and pharmaceutical research were early users of the new technology. A more recent and rapidly developing area is the study of homogeneous catalysis in solution via ESI-MS, and this involves the detection of ionic catalytic intermediates [1]. This is the central area of the present book.

The significance of ESI-MS was recognized by the award of a Nobel Prize in 2002 to John Fenn [2], who was the major developer of the method. The initial development of the method is due to Malcolm Dole. In the nineteen sixties Malcolm Dole was interested in the determination of the molecular mass of synthetic polymers. But how could one get large polymers into the gas-phase without decomposing them? Dole reasoned that if one used a very dilute solution of the analyte and nebulized such a solution into extremely small droplets one could obtain many droplets that contain only a single analyte molecule. Evaporation of such droplets would then lead to a transfer of the analyte molecules to the gas phase. If the analyte was

not charged, as was the case for some polymers, the presence of an electrolyte such as $Na^+$ could lead to addition of $Na^+$ to the polymer molecule on evaporation of droplets that happen to contain a single polymer molecule and one $Na^+$ ion. Such statistical charging was known to occur [3] but was a rather inefficient source of ionized analytes. Something better was required. While working as a consultant of a paint company, Dole witnessed the use of electrostatic spraying to apply paint to car bodies [4a]. In this spray process, the spray nozzle was kept at a high voltage, and this led to the production of very small charged paint droplets which were attracted to the car body kept at ground potential. Dole and coworkers were able to produce small charged droplets by applying electrospray to polystyrene solutions. The evaporation of the very small droplets led to polystyrene ions that could be detected using ion mobility or kinetic energy analysis of the produced ions [4b]. While Dole's methods and results had some flaws they clearly indicated that electrospray is a very promising soft ionization method for macromolecules [4b].

Following Dole's [4] work, John Fenn introduced some decisive improvements that allowed a mass spectrometer to be interfaced to an electrospray source [5, 6] and clearly demonstrated that ESI-MS could be used very effectively for the analysis of small ions and molecules [5] as well as peptides and proteins with a molecular mass extending into the megadalton range [6]. This work had a big impact and started the ESI-MS revolution that is continuing to this day.

1.1.2
**Aims of this Chapter**

This chapter is written for users of ESI-MS. It presents an account of 'how it all works.' Such understanding is desirable because the observed mass spectra depend on a large number of parameters. These start with a choice of solvent and concentrations of the analyte, choice of additives to the solution that may be beneficial, choice of the flow rates of the solution through the spray capillary, the electrical potentials applied to the spray capillary (also called 'needle') and the potentials of ion optical elements that are part of the mass analyzer. Proper choice of these parameters requires not only some understanding of conventional mass spectrometry but also of the electrospray mechanism. In early work on ESI-MS many of these parameters were established by trial and error, but now that a better understanding of the mechanism is at hand more rational choices are possible. The present chapter provides an up to date account of Electrospray. For a broader coverage, which is somewhat dated but still relevant, the review by Smith and coworkers is recommended [7].

As mentioned already, electrospray existed long before its application to mass spectrometry. It is a method of considerable importance for the electrostatic dispersion of liquids and creation of aerosols. Much of the theory concerning the mechanism of the charged droplet formation was developed by researchers in aerosol science. A compilation of articles devoted to electrospray can be found in a recent special issue of the Journal of Aerosol Science [8].

## 1.2
## Production of Gas-Phase Ions by Electrospray and Electrospray Ionization Mass Spectrometry

### 1.2.1
### Overview

There are three major steps in the production of gas-phase ions from electrolyte ions in solution: (a) production of charged droplets at the ES capillary tip; (b) shrinkage of the charged droplets due to solvent evaporation and repeated charge-induced droplet disintegrations that ultimately lead to small highly charged droplets capable of producing gas-phase ions, and (c) the actual mechanism by which gas-phase ions are produced from these droplets. All stages occur in the atmospheric pressure region of the apparatus, see Figure 1.1.

A small fraction of the ions resulting from the preceding stages enter the vacuum region of the interface leading to the mass spectrometer through a small orifice or capillary. Two types of apparatus using a capillary are shown in Figure 1.2. The created gas-phase ions may be clustered with solvent molecules and other additives that
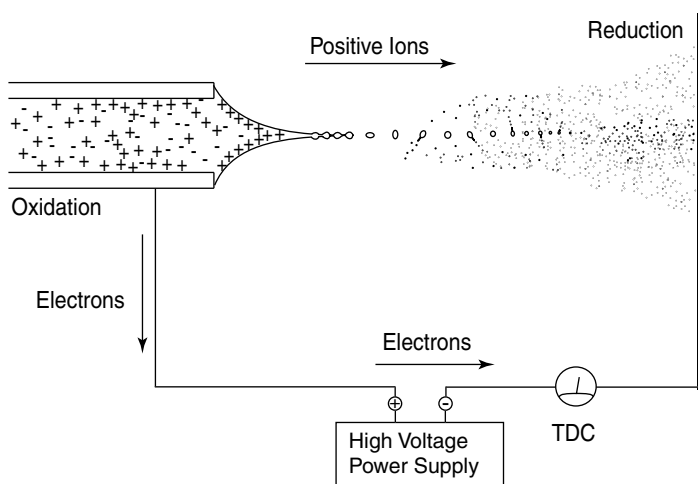


**Figure 1.1** Schematic of major processes occurring in the atmospheric pressure region of electrospray. TDC stands for total droplet current (*I*). The figure illustrates major processes occurring in the atmospheric pressure region of an ESI run in the positive ion mode. Penetration of the imposed electric field into the liquid leads to formation of an electric double layer at the meniscus. The double layer is due to the polarizabilty and dipole moments of the solvent molecules and an enrichment near the meniscus of positive ions present in the solution. These cause a destabilization of the meniscus and formation of a cone and a jet charged by an excess of positive ions. The jet splits into droplets charged with an excess of positive ions. Evaporation of the charged droplets brings the charges closer together. The increasing Coulombic repulsion destabilizes the droplets, which emit a jet of smaller charged progeny droplets. Evaporation of progeny droplets leads to destabilization and emission of a second generation of progeny droplets, and so on until free gas-phase ions form at some point.

(a)



(b)
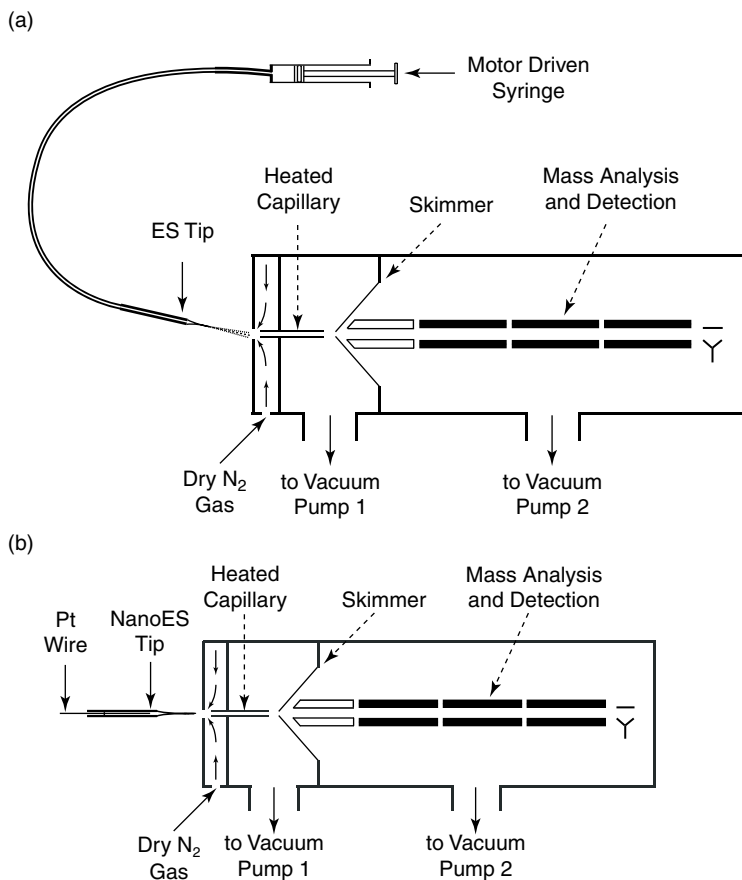


**Figure 1.2** (a) Schematic of Electrospray (ES) and interface to mass spectrometer. Solution containing analyte is supplied to the ES spray tip by a motor-driven syringe via flexible glass capillary tubing. A positive potential is applied to the spray tip (positive ion mode). The spray of positively charged droplets emerges from the spray capillary tip (see Figure 1.1). Solvent evaporation of the charged droplets leads to gas-phase ions. A mixture of ions, small charged droplets, and solvent vapor in the ambient gas enters the orifice leading to the nitrogen counter-current chamber. The weak nitrogen counter-current removes the solvent vapor, but the ions, driven by an electric potential and pressure difference, enter the heated capillary pathway into the low pressure chamber. An electric field between this capillary and the skimmer cone accelerates the ions for a further collision-activated 'clean-up' of the ions. The potential difference over the cone orifice and downstream ion optical elements transports the ions into the high vacuum region of the mass analysis chamber. (b) Same as Figure 1.2a but showing Nanoelectrospray. Large diameter end of NanoES tip capillary is 'loaded' with µL amounts of solution. The electrical potential is supplied to the nano tip either by a Pt wire or by a metal film coating the outside of the capillary. A spray of charged nano droplets results from the pull of the electric field on the polarized meniscus of the solution at the capillary tip.

would broaden $m/z$ peaks excessively. The gas-phase ions are therefore subjected to a *thermal* declustering or 'clean-up' stage by heating the capillary. Often a countercurrent flow of an inert gas is used to minimize entrance of solvent vapor into the vacuum region. A second clean-up stage is obtained through *collisional*

activation by applying an electric potential difference between the capillary exit and the skimmer. The chamber past the capillary is at a vacuum of a few torr, so that acceleration of ions by the applied field results in multiple collisions with neutral gas molecules. The accumulating internal energy of the ions leads to ion desolvation, and at higher applied fields to ion fragmentation. The mass-selecting ion optics of the mass spectrometer are placed beyond the skimmer because they require high vacuum conditions.

### 1.2.2
### Production of Charged Droplets at the Capillary Tip

As shown in Figure 1.1, a voltage ($V_c$) of 2–3 kV is applied to the spray capillary. The counter electrode in ESMS may be a plate with an orifice leading to the mass spectrometric sampling system or a sampling capillary, mounted on the plate, which leads to the MS, as shown in Figure 1.2a. Because the spray capillary tip has a very small diameter, the electric field ($E_c$) at the capillary tip is very high ($E_c \approx 10^6$ V/m). The value of the field at the capillary tip opposite a large and planar counter electrode can be evaluated with the approximate relationship [9];

$$E_c = 2 \, V_c/[r_c\ln(4d/r_c)] \tag{1.1}$$

where $V_c$ is the applied potential, $r_c$ is the capillary outer radius, and $d$ is the distance from the capillary tip to the counter electrode. For example, the combination of $V_c = 2000$ $V$, $r_c = 5 \times 10^{-4}$ m and $d = 0.02$ m leads to: $E_c \approx 1.6 \times 10^6$ V/m. As indicated by Eq. (1.1) the field $E_c$ is proportional to $V_c$, with the most important geometry parameter being $r_c$. $E_c$ is essentially inversely proportional to $r_c$, while it decreases slowly with the electrode separation $d$.

A typical solution supplied to the capillary is a polar solvent in which the analyte is soluble. Because ESI-MS is a very sensitive method, low concentrations, $10^{-7} - 10^{-3}$ mol L$^{-1}$ ($M$), of analyte need to be used. Methanol or methanol/water, acetonitrile or acetonitrile/water are often used as the solvent. However, apolar and nonprotic solvents like toluene, nitromethane, dichloromethane and formamide can be used as well although ionic additives may be required in order to obtain stable spray conditions. For an overview of some of the solvents used in electrospray see Ref. [10]. For simplicity in the subsequent discussion, we will assume that the analyte is ionic, and only the positive ion mode will be considered.

The field $E_c$ when turned on, will penetrate the solution near the spray capillary tip. This will cause a polarization of the solvent near the meniscus of the liquid. In the presence of even traces of an electrolyte, the solution will be sufficiently conducting and the positive and negative electrolyte ions in the solution will move under the influence of the field. This will lead to an enrichment of positive ions on or near the surface of the meniscus and enrichment of negative ions away from the meniscus. The forces due to the polarization cause a distortion of the meniscus into a cone pointing downfield (see Figure 1.1). The increase of surface due to the cone formation is resisted by the surface tension of the liquid. The cone formed is called a Taylor cone (see Taylor [11] and Fernandez de la Mora [12]). If the applied field is sufficiently high,

(a)  (b)  (c)
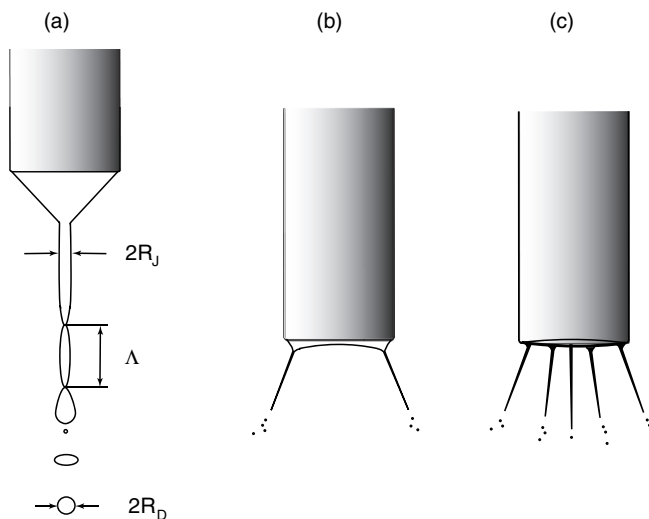


**Figure 1.3** Different forms of Electrospray at the tip of the spray capillary. (a) cone jet mode. Relationship between radius of droplets and radius of jet: $R_D/R_J \approx 1.9$. (b) and (c). Multijet modes result as the spray voltage is increased, and the flow rate imposed by the syringe is high. (After Cloupeau, Ref. [13].)

a fine jet emerges from the cone tip, whose surface is charged by an excess of positive ions. The jet breaks up into small charged droplets (see Figure 1.1 and Figure 1.3a, due to Cloupeau [13a]).

It is apparent from Figure 1.3a that the size of the droplets formed from the cone jet is dependent on the jet diameter $2R_J$. The droplets initially produced therefore could be expected to be approximately of the same size. This was proposed by Cloupeau [13] and confirmed by studies of Tang and Gomez [14]. The formed droplets are positively charged because of an excess of positive electrolyte ions at the surface of the cone and the cone jet. Thus, if the major electrolyte present in the solution is ammonium acetate, the excess positive ions at the surface will be $NH_4^+$ ions. This mode of charging, which depends on the positive and negative ions drifting in opposite directions under the influence of the electric field, has been called the electrophoretic mechanism [13b,c].

The charged droplets drift downfield through the air toward the opposing electrode. Solvent evaporation at constant charge leads to droplet shrinkage and an increase in the repulsion between the charges. At a given radius, the increasing repulsion overcomes the surface tension at the droplet surface. This causes a coulomb fission (also called a coulomb explosion) of the droplet. The droplet fission occurs via formation of a cone and a cone jet that splits into a number of small progeny droplets. This process bears a close resemblance to the cone jet formation at the capillary tip (see de la Mora [12] and references therein). Further evaporation of the parent droplet leads to repeated fissions. The progeny droplets also evaporate

and break up. Very small charged droplets result that ultimately lead to gas-phase ions by processes which will be described in detail in subsequent sections.
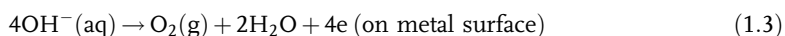
The cone-jet mode at the spray capillary tip described and illustrated in Figures 1.1 and 1.3a is only one of the many possible ES modes. For a qualitative description of this and other modes, see Cloupeau [13a–c]. More recent studies by Vertes and coworkers [15] using fast time-lapse imaging of the Taylor cone provide details on the evolution of the Taylor cone into a cone jet and pulsations of the jet. These pulsations lead to spray current oscillations. The current oscillations are easy to determine with conventional equipment and can be used as a guide for finding conditions that stabilize the jet and improve signal-to-noise ratios of the mass spectra. The cone-jet mode is the most used and best characterized mode in the electrospray literature [12, 13].

The magnitude of currents obtained with ES (see Figure 1.1) in the cone jet mode at a typical flow rate of $6\,\mu L/min$ are around $0.1\,\mu A$. Only a fraction of this current will enter the first chamber after passage through the heated capillary and skimmer (see Figures 1.1 and 1.2). A charge loss by a factor of 100 would reduce the ion current to $10^{-9}$ A; fortunately, modern current detection technology employing ion-electron multipliers allows the detection of much lower currents typically in the range of $10^{-12} - 10^{-16}$ A.

### 1.2.3
### Electrospray as an Electrolytic Cell

At a steady operation of the electrospray in the positive ion mode (see Figure 1.1), the positive droplet emission continuously carries off positive charge. The requirement for charge balance together with the fact that only electrons can flow through the metal wire that supplies the electric potential to the electrodes (Figure 1.1) leads to the conclusion that the ES process must include an electrochemical conversion of ions to electrons. In other words, the ES device can be viewed as a special type of electrolytic cell [16]. It is special because the ion transport does not occur through uninterrupted solution, as is normally the case in electrolysis, but through the gas phase. Thus, in the positive ion mode where the charge carriers are positively charged droplets (and subsequently gas-phase positive ions) a conventional electrochemical oxidation reaction should be occurring at the positive electrode, that is at the liquid/metal interface of the spray capillary (Figure 1.1). This reaction replenishes positive ions to the solution and prevents the build-up of a charge imbalance. Concurrently, gas-phase ions are reduced when they hit a downstream metal surface. The nature of these ions depends on the experimental conditions. If the spray capillary is made of metal (M), the metal can become oxidized and enter the solution as cations, while releasing electrons to the metal electrode, see Eq. (1.2).

$$M(s) \rightarrow M^{2+}(aq) + 2e \text{ (on metal surface)} \tag{1.2}$$

$$4OH^-(aq) \rightarrow O_2(g) + 2H_2O + 4e \text{ (on metal surface)} \tag{1.3}$$

The other alternatives for restoring the charge balance are the removal of negative ions present in the solution by an oxidation reaction as illustrated in Eq. (1.3)

(for aqueous solutions) or oxidation of sacrificial additives such as $I^-$ or hydroquinone [17, 18].

One expects that the reaction with the lowest oxidation potential will dominate, and that the oxidation reaction will be dependent on the material present in the metal electrode, the solutes/ions present in the solution, and the nature of the solvent. Proof of the occurrence of an electrochemical oxidation at the metal capillary was provided by Blades *et al.* [16]. When a Zn spray capillary tip was used, release of $Zn^{2+}$ to the solution could be detected. Furthermore, the amount of $Zn^{2+}$ release to the solution per unit time when converted to coulomb charge per second was found to be equal to the measured electrospray current (*I*) in amperes (coulomb/s, Figure 1.1). Similar results were observed with stainless steel capillaries [16]. These were found to release $Fe^{2+}$ to the solution. These quantitative results provided the strongest evidence for the electrolysis mechanism. These oxidation reactions introduce ions which were not previously present in the solution (see Eq. (1.2)). However, they also provide an opportunity to generate reactive intermediates that can be studied by mass spectrometry.

Van Berkel and coworkers have examined the consequences of the electrochemical processes to ESI-MS in a series of publications [17]. They were able to demonstrate that ions produced by the electrolysis process can in some cases have unintended and undesired effects on the mass spectra obtained with pH- or oxidation-sensitive analytes [17].

Ions introduced into the solution by inadvertent or deliberate electrolysis amount to very low concentrations. Taking the Zn capillary tip as example, a solution of $10^{-5}$ M NaCl in methanol at a flow rate $V_f = 20 \, \mu L \, min^{-1}$ was found to lead to an electrospray current of $1.6 \times 10^{-7}$ A. The $Zn^{2+}$ concentration produced by the Zn-tipped capillary evaluated from the current was $2.2 \times 10^{-6}$ M. Assuming that the $Na^+$ ion was the analyte ion, the concentration of the ions produced by the oxidation at the electrode is only $\sim 1/5$ of that of the analyte. It will be shown later that the electrospray current increases very slowly with the total electrolyte concentration. Therefore, ions produced by oxidation at the electrode may not be noticed in the mass spectrum at higher analyte or additive concentrations.

### 1.2.4
### Required Electrical Potentials for ES. Electrical Gas Discharges

D.P.H. Smith [19] was able to derive a useful approximation for the electric field at the capillary tip ($E_{on}$) required for the *onset* of instability of a static Taylor cone, see Eq. (1.4). Instability of the Taylor cone is required for the formation of a jet at the apex of the cone. The equation for the onset field, when combined with Eq. (1.1), leads to an equation (for the potential, $V_{on}$, required for the start of electrospray;

$$E_{on} \approx \left( \frac{2\gamma \cos \theta}{\varepsilon_o r_c} \right)^{1/2} \tag{1.4}$$

$$V_{on} \approx \left( \frac{r_c \gamma \cos \theta}{2\varepsilon_o} \right)^{1/2} \ln(4d/r_c) \tag{1.5}$$

**Table 1.1** Onset voltages[a], $V_{on}$ for ESI of solvents with different surface tension $\gamma$.

| Solvent | CH$_3$OH | CH$_3$CN | (CH$_3$)$_2$SO | H$_2$O |
|---|---|---|---|---|
| $\gamma$ (N m$^{-1}$) | 0.0226 | 0.030 | 0.043 | 0.073 |
| $V_{on}$ (Volt) | 2200 | 2500 | 3000 | 4000 |

[a]Calculated with Eq. (1.6).

where $\gamma$ is the surface tension of the solvent, $\varepsilon_o$ is the permittivity of vacuum, $r_c$ is the radius of the capillary, and $\theta$ is the half angle for the Taylor cone. Substituting the values $\varepsilon_o = 8.8 \times 10^{-12}$ J$^{-1}$ C$^2$ and $\theta = 49.3$ (see Taylor [11]), one obtains

$$V_{on} = 2 \times 10^5 (\gamma r_c)^{1/2} \ln(4d/r_c) \tag{1.6}$$

where $\gamma$ must be substituted in N/m and $r_c$ in m to obtain $V_{on}$ in volts. Shown in Table 1.1 are the surface tension values for four solvents and the calculated electrospray onset potentials for $r_c = 0.1$ mm and $d = 40$ mm. The surface of the solvent with the highest surface tension (H$_2$O) is the most difficult to stretch into a cone and jet, and this leads to the highest value for the onset potential $V_{on}$. As a result, use of neat water as solvent can lead to the initiation of an electric discharge from the spray capillary tip.

Experimental verification of Eqs. (1.5) and (1.6) has been provided by Smith [19], Ikonomou *et al.* [20] and Wampler *et al.* [21] For *stable* ES operation one needs to go a few hundred volts higher than the calculated $V_{on}$. The electrospray onset potential is the same for both the positive and negative ion modes, but the electric discharge onset is lower when the capillary electrode is negative [19, 20] and metallic. This is probably due to emission of electrons from the negative capillary, which initiate the discharge. Use of glass capillaries reduces the risk of electric discharge. In this case the electric potential is applied via an internal metal wire or external metal coating in contact with the solution (see Figure 1.2b). Neat water as solvent can be used with this 'nanospray' arrangement without the occurrence of electric discharges.

The occurrence of electric discharge leads to a sudden increase in the ion current together with a visible glow around the spray capillary [22]. Currents above $10^{-6}$ A are generally due to the presence of an electric discharge. A more specific test is provided by the appearance of discharge-characteristic ions in the mass spectrum. Thus, in the positive ion mode the appearance of protonated solvent clusters such as H$_3$O$^+$(H$_2$O)$_n$ from water or CH$_3$OH$_2^+$(CH$_3$OH)$_n$ from methanol solvent indicates the presence of a discharge [20]. In the absence of an electrical discharge, protonated solvent ions are only produced at high abundance when the solvent has been acidified, that is when H$_3$O$^+$ or CH$_3$OH$_2^+$ are present in the solution. The presence of an electrical discharge severely degrades the performance of ESMS. The electrospray ions are observed at much lower intensities than was the case prior to the discharge, while discharge-generated ions appear with very high intensities [20, 21].

Air at atmospheric pressure is not only a convenient but also a very suitable ambient gas for ES, particularly when solvents with high surface tension are to be

electrosprayed. Initiation of gas discharges occurs when free electrons are accelerated by the high electric field near the capillary to velocities where they can ionize the gas molecules. At near atmospheric pressures, the collision frequency of the electrons with the gas molecules is very high, limiting the electron acceleration process and minimizing the initiation of an electric discharge. In addition to the pressure effect, oxygen molecules in air have electron affinity and readily capture free electrons. Trace gases such as $SF_6$, with higher electron affinity and electron capture cross sections than $O_2$, can be added to assist the electron capture and suppress the electrical breakdown at higher electrospray voltages, when the atmospheric oxygen effect is insufficient [21].

### 1.2.5
### Current, Charge and Radius of Droplets Produced at the Capillary Tip

Fernandez de la Mora and Locertales [23] have proposed the following approximate relationships that correlate the current, droplet size and charge on the generated droplets. Assuming a flow rate below $1\,\mu L\,min^{-1}$ and operation of electrospray in the *cone jet mode,*

$$I = f\left(\frac{\varepsilon}{\varepsilon_o}\right)\left(\gamma K V_f \frac{\varepsilon}{\varepsilon_o}\right)^{1/2} \tag{1.7}$$

$$R \approx (V_f \varepsilon / K)^{1/3} \tag{1.8}$$

$$q \approx 0.7[8\pi(\varepsilon_o \gamma R^3)^{1/2}] \tag{1.9}$$

where $\gamma$ is the surface tension of solvent; $\varepsilon$ the permittivity of solvent; $\varepsilon_o$ the permittivity of vacuum (free space); the $\varepsilon/\varepsilon_o$ ratio the dielectric constant of solvent; $K$ the conductivity of solution; $E$ the applied electric field at capillary tip (see Eq. (1.2)); $R$ the radius of droplets produced at capillary tip; $q$ the charge of droplets and $V_f$ the flow rate (volume/time); $f(\varepsilon/\varepsilon_o)$ is a numerical function tabulated by the authors [23]. For liquids with a dielectric constant $(\varepsilon/\varepsilon_0) \geq 40$ (water, water/methanol mixtures, acetonitrile, formamide) the value of $f(\varepsilon/\varepsilon_o)$ is approximately 18. The described relationships were obtained for solutions with a conductivity larger than $10^{-4}\,S\,m^{-1}$. Assuming electrolytes that dissociate completely, this requirement corresponds to solutions with concentrations higher than $\sim 10^{-5}\,mol\,L^{-1}$, that is a concentration range commonly present in ESMS. A more recent theoretical treatment by Cherney [24] has confirmed the deductions of Fernandez de la Mora and Locertales and has provided a more detailed description of the conditions existing in the cone jet. The derived relationships are also in agreement with experimental data by Chen and Pui [25].

### 1.2.6
### Solvent Evaporation from Charged Droplets Causes Coulomb Fissions of Droplets

The charged droplets produced by the spray needle shrink due to solvent evaporation while the charge remains constant. As the droplet gets smaller, the repulsion between

the charges at the surface increases and at a certain droplet radius the repulsion of the charges overcomes the cohesive force of the surface tension. This instability results in fission of the droplet, at which point the droplet typically releases a jet of small, highly charged, progeny droplets. The condition for the instability is given by the Rayleigh [26] equation;

$$Q_{Ry} = 8\pi(\varepsilon_0\gamma R^3)^{1/2} \tag{1.10}$$

where $Q_{Ry}$ is the charge on the droplet; $\gamma$ is the surface tension of the solvent; $R$ is the radius of the droplet and $\varepsilon_o$ is the electrical permittivity. The fission at or near the Rayleigh limit, with release of a jet of small monodisperse charged progeny droplets, has been confirmed by a number of experiments.

Most experiments used Phase Doppler Interferometry (PDI), a method well suited for volatile solvents as used in ESI-MS [27]. A series of PDI measurements using various solvents are given in Table 1.2. One can deduce from this table that the dependence on the type of solvent is relatively small. Thus, droplets from all solvents experience Coulomb fissions close to, or at, the Rayleigh limit. The loss of mass on fission is between 2 and 5% of the parent droplet mass but the loss of charge is much larger, that is, some 15–25% of the charge of the parent droplet.

Beauchamp and coworkers [28] provide information on the charge of the parent droplet immediately after the droplet fission. An example of such data is given in Figure 1.4, where the charge of the droplets before and after the fission is given as a percentage of the Rayleigh condition, Eq. (1.10). These, and results for the other solvents studied [28], show that the evaporating charged droplets oscillate at all times between fairly narrow limits of the Rayleigh condition. This finding has a bearing on the discussion of the mechanism by which large molecules enter the gas phase (see the Charged Residue Mechanism in Section 1.2.10). Notable also, see Figure 1.4a, is the observation that the diameter of the charged parent droplet undergoing evaporation *and* Coulomb fissions remains very close to the diameter of an uncharged droplet that loses mass solely because of evaporation. This result supports the observations of a series of authors (see Table 1.2 and Refs. [26, 29–31]).

When the sprayed solution contains a solute, such as a salt, the continuous evaporation of the droplets will lead to very high concentrations of the salt and finally to charged solid particles – 'skeletons' of the charged droplets that can reveal some aspects of the droplet evolution. Fernandez de la Mora and coworkers [32] have used this approach to study charged droplet evolution. This work is of special relevance to the ion evaporation model and is discussed in Section 1.2.8.

### 1.2.7
**Evaporation of Droplets Leading to Coulomb Fissions Producing Progeny Droplets that Ultimately Lead to Ions in the Gas-Phase; Effects of the Concurrent Large Concentration Increase**

It is clear that the process of repeated droplet fissions of both parent and progeny droplets ultimately will lead to very small charged droplets that are the precursors of the gas-phase ions. The mechanisms by which the gas-phase ions are produced from

**Table 1.2** Experimental observations of Rayleigh fissions of charged droplets.

| Reference | Solvent | Droplet diameter range (μm)[a] | Onset of Instability (% of Rayleigh limit) | % of mass lost in breakup[a] | % of charge lost in breakup |
|---|---|---|---|---|---|
| (Smith *et al.* Ref. [28a]) | Water | 10–40 | 90 | nd | 20–40 |
| | Methanol | 10–40 | 110 | nd | 15–20 |
| | Acetonitrile | 10–40 | 100 | nd | 15–20 |
| (Grimm and Beauchamp Ref. [28b]) | *n*-Heptane | 35–45 | 100 | nd | 19 |
| | *n*-Octane | | 87 | nd | 17 |
| | *p*-Xylene | | 89 | nd | 17 |
| (Gomez and Tang Ref. [27]) | Heptane | 20–100 | 70 | nd | nd |
| (Taflin *et al.* Ref. [29]) | Low vapor pressure oils | 4–20 | 75–85 | 2 | 10–15 |
| (Richardson *et al.* Ref. [30]) | Dioctyl phthalate | nr | 102–84 | 2.3 | 15–50 |
| (Schweitzer *et al.* ref. [31]) | n-octanol | 15–40 | 96–104 | 5 | 23 |

[a]nr: not reported, nd: not determined.

(a)



(b)
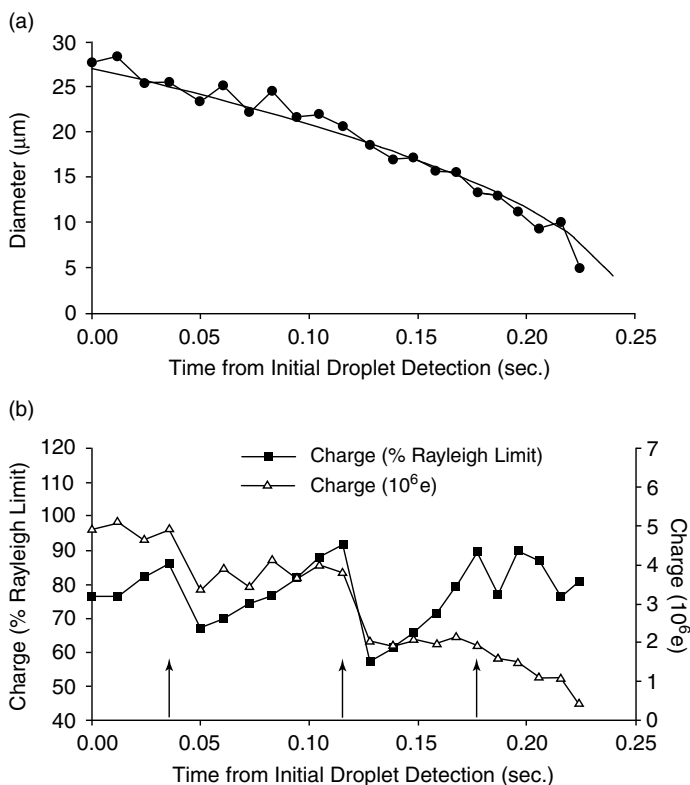


**Figure 1.4** Evaporation and discharge of a positively charged water droplet in nitrogen gas at ambient pressure and 317 K and a weak ($51\,V\,cm^{-1}$) electric field. (a) Variation of droplet diameter with time. Also plotted (smooth curve) is the predicted change in diameter due to evaporation of a neutral water droplet in a vapor-free $N_2$ gas at 317 K. (b) Variation of droplet charge with time, represented as number of elementary charges and as percent of the Rayleigh limit. Arrows indicate discharge events. Note that water droplets undergo a Coulomb fission at approximately 90% of the Rayleigh limit and are at approximately 65% of the limit after the Coulomb fission. (Reprinted from Ref. [28a] with permission from the American Chemical Society.)

the very small 'final' droplets is considered in Sections 1.2.8 and 1.2.10. Here we examine some of the details of the evolution of the initial droplets formed at the spray capillary. The whole process is driven by the decrease in droplet volume by solvent evaporation. The continuous evaporation is possible because the thermal energy required for the evaporation is provided by the ambient gas at near atmospheric pressure. As will be shown below, a large loss of solvent by evaporation occurs before the final droplets are formed that lead to ions. It is instructive and for certain applications desirable to estimate the increase in solute concentration due to the volume lost by evaporation.

A droplet evolution scheme is shown in Figure 1.5. It deals with droplets produced by nanoelectrospray. Nanospray (see Section 1.2.4) is a technique that considerably

Charge number $Z$
Radius (µm)    R
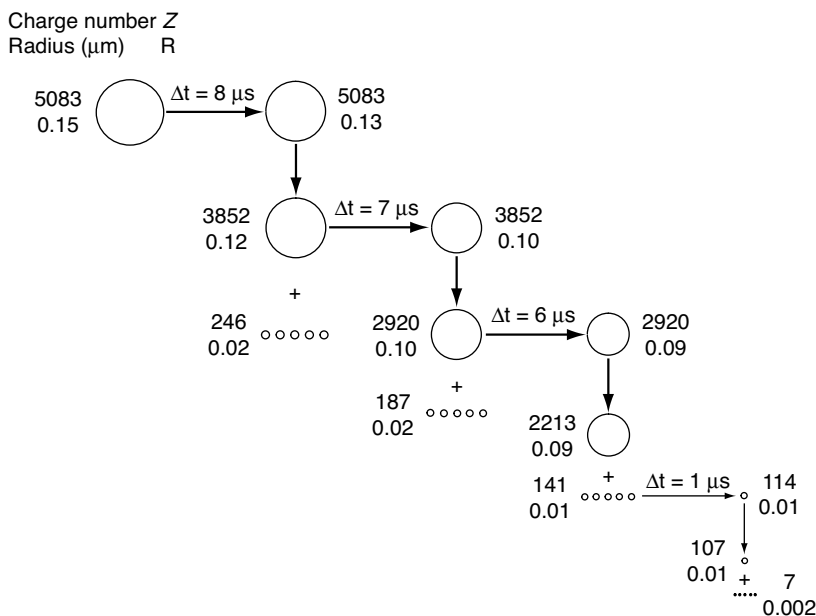


**Figure 1.5** Droplet history of charged water droplets produced by nanospray. First droplet is one of the droplets produced at spray needle. This parent droplet is followed over three evaporation and fission events. The first generation progeny droplets are shown as well as the fission of one of the progeny droplets that leads to second-generation progeny droplets. $R$ is the radius of the droplets and $Z$ gives the number of charges on the droplet. $Z$ corresponds to the number of excess singly charged ions near the surface of the droplet. The parent's charge is $Z = 0.9 \ Z_R$ just before the fission and $Z = 0.7 \ Z_R$ just after the fission (as observed in Figure 1.4), while the progeny droplets have $Z = 0.7 \ Z_R$ just after the fission of the parent. (Based on Figure 1.1 in Peschke, Verkerk and Kebarle [33].) It should be noted that the droplets' history presented in Figure 1.6 is only a qualitative model. Thus, the assumption that only five progeny droplets could be formed at each fission is quite uncertain. The actual number could be much larger and the progeny droplets much smaller.

reduces the droplet diameter by performing electrospray using a glass capillary. Because the charged droplets are very much smaller than the droplets produced by electrospray, these droplets reach the final droplet stage much sooner.

In deriving Figure 1.5, the used stability limits for droplet fission (at droplet charge $Z = 0.9 \ Z_R$) and droplet charge just after the droplet fission ($Z = 0.7 \ Z_R$) were due to Beauchamp and coworkers [28a]. Further assumptions with which Figure 1.5 was obtained are described in the section 'Calculations and Experimental' of Peschke *et al.* [33]. Using the droplet radii, one can calculate that approximately 40% of the volume is lost *between* each fission, while only 2–5% of the parent droplet mass is lost *in* each fission event. This means that after 10 successive fissions of the parent droplet a 29-fold volume decrease will have taken place corresponding to a 29-fold solute concentration increase in the parent droplet. Such very large increases in concentration will promote the occurrence of undesired bimolecular reactions, like ion pairing, involving analyte ions and impurities present in the solution, see Section 1.2.12.

1.2.8

## Mechanism for the Formation of Gas-Phase Ions from Very Small and Highly Charged Droplets. The Ion Evaporation Model (IEM)

Two mechanisms have been proposed to account for the formation of gas-phase ions from the final droplets. The first mechanism was proposed by Dole [4], who was interested in analytes of very high molecular mass (see introduction). For such macromolecules, droplet evolution as described in the preceding section would lead to some droplets containing one analyte molecule in addition to the ionic charges on the surface of the droplet. Solvent evaporation from such a droplet will lead to a gas-phase analyte ion whose charge originates from the charge at the surface of the vanished droplet. This assumption is now known as the Charged Residue Model (CRM) and is discussed in detail in Section 1.2.10.

Iribarne and Thomson [34], who worked with small ionic analytes such as $Na^+$ and $Cl^-$, proposed a second mechanism, the Ion Evaporation Model (IEM). This model predicts that, after the radii of the droplets have decreased to a very small size ($\leq 10$ nm), direct ion emission from the droplets will occur. At this point, the *ion evaporation* process replaces Coulomb fission. Iribarne and Thomson supported their model by experimental [34a] and theoretical [34b] results. The experimental results involved measurements of the relative abundance of the ions produced by ESI of solutions containing NaCl as the only solute. The authors found that there was a large number of ion aggregates of the type $[(NaCl)_n(Na)_m]^{m+}$, including $[(NaCl)_n(Na)]^+$, whose abundance decreased rapidly as $n$ increased. However, the ion with lowest mass in that series, $Na^+$, ($n = 0$, $m = 1$), and hydrated $Na(H_2O)_k^+$ ($k = 1$–3) had the highest abundances by far. While the large aggregate ions produced by ESI are probably due to a charged residue mechanism type process, the abundant $Na^+$ and $Na^+$ hydrates must be produced by a different mechanism. Iribarne and Thomson proposed a direct escape of $Na^+$ charges from the surface of the multiply charged droplets. This process begins to occur after the droplets reach a very small size. Once ion evaporation sets in, there are no more droplet fissions because the excess charges on the droplets are removed by ion evaporation.

The authors also developed theoretical equations for the droplet conditions that will lead to ion evaporation based on Transition State Theory as used in reaction kinetics [34b]. Assuming that the evaporating ion is one of the ionic charges at the surface of the droplet, the leaving ion is *repelled* by the Coulomb repulsion between it and the remaining charges on the droplet at increasing charge separation. But at very short distances from the droplet an *attractive* force between the leaving ion and the droplet is present as a result of the polarization of the droplet induced by the leaving ion. The ion-polarizability attraction is larger at very short distances from the droplet surface, while the repulsion becomes dominant at larger distances. The transition state is located where these two interactions become equal. The graphs in Figure 1.6 show the predicted radius at which droplet fission at the Rayleigh limit is replaced by ion evaporation. It indicates that the charged droplets must reach a radius of approximately 100 Å (10 nm) before ion evaporation replaces droplet fission.
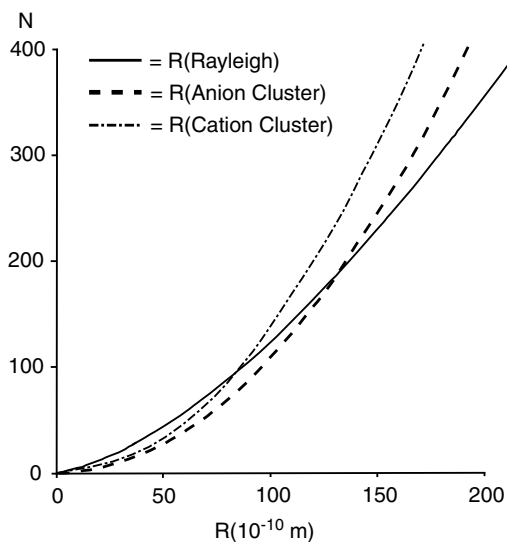
**Figure 1.6** Predictions of the ion evaporation theory [34]. The Rayleigh curve provides the droplet radius *R* and the number of elementary charges *N* at which a charged water droplet will be at the Rayleigh limit. Solvent evaporation at constant charge to a smaller radius *R* will cause a Coulomb fission. Similarly, the curves Cation Cluster and Anion Cluster show the threshold of ion evaporation at a given charge *N* and droplet radius *R*. For negatively charged droplets, moving at constant charge to a smaller radius *R* due to solvent evaporation will lead to negative ion evaporation when the radius $R = 140 \, \text{Å}$, ($1 \, \text{nm} = 10 \, \text{Å}$) and for positively charged droplets at $R = 84 \, \text{Å}$, where the ion evaporation (Cation Cluster) and Rayleigh curves cross. Below this radius, ion evaporation replaces Coulomb fission. Thus, taking a radius of $R \approx 100 \, \text{Å}$ provides a useful benchmark for the region where ion evaporation takes over.

Several research groups have performed experiments to examine the predictions of the theory. Some of the most relevant work is due to Fernandez de la Mora and coworkers [32], who used an interesting approach to provide strong evidence for the qualitative validity of the ion evaporation mechanism. Instead of concentrating on the evaporating droplets, they focused on the sizes and charges of the solid residues formed after complete evaporation of the solvent from the droplets. Since the solid residues had been 'charged droplets' before the last of the solvent evaporated, the size and charge of these residues should represent to a fair approximation the sizes and charges of the final charged droplets. The solid residues representing final droplets frozen in time are amenable to measurement. This approach provided results that were in good agreement with IEM [32].

Theoretical work involving simulations of ion evaporation from charged droplets can also provide valuable insights into IEM. A good example is the work by Vertes and coworkers [35] on the evaporation of $H_3O^+$ ions from charged water droplets. The authors used classical molecular dynamics simulations to study droplets of 6.5 nm diameter. Checks were made that the parameters used led to predictions of properties (such as the radial distribution function, the enthalpy of evaporation and the self diffusion coefficients) that are in agreement with experimental values.

Droplets of 6.5 nm diameter, which consist of some 4000 water molecules, were charged with $H_3O^+$ ions; ion pairs corresponding to a dissolved solute were not added. Remarkably, not all $H_3O^+$ ions were located on the surface of the droplet at equilibrium as is generally assumed for IEM. As $H_3O^+$ charges were added, fluctuations of water molecules at the droplet surface became much more pronounced. Some of these fluctuations developed into large protuberances that separated as hydrated $H_3O^+$ ions. Generally the 'solvation shell' of the departing $H_3O^+$ consisted of some 10 water molecules. Interested readers can observe the simulation of such ion evaporation at the website of Vertes (see http://www.gwu.edu/~vertes/publicat.html).

In summary, the Ion Evaporation Model is experimentally well supported for small ions of the kind that one encounters in inorganic and organic chemistry. However, when the ions become very large, such as polymers, dendrimers or biological supramolecular complexes like proteins and enzymes, the Charged Residue Model (CRM) becomes much more plausible, see Section 1.2.10. Because many applications of ESMS in analytical organometallic and physical organic chemistry involve small ions it is desirable to consider the expected relative sensitivities for these analytes when detected with ESMS.

### 1.2.9
### Observed Relative Ion Intensity of Small Analytes. Dependence on the Nature of the Analyte, its Concentration and Presence of Other Electrolytes in the Solution. High Sensitivities of Surface-Active Analytes

The dependence of the sensitivities of ionic analytes on the nature of the analyte, its concentration, and the presence of other electrolytes in solution is of interest to users of electrospray mass spectrometry. The analytes considered in this section are smaller molecules that most likely enter the gas phase via the Ion Evaporation Model (IEM).

The dependence of the total droplet current produced at the spray capillary on various parameters was given in Eq. (1.7). Relevant to the present discussion is the dependence of the current ($I$) on the square root of the conductivity of the solution. At the low total electrolyte concentrations generally used in ESI, the conductivity is proportional to the concentration of the electrolyte. Thus, if a single electrolyte (E) was present in the sprayed solution, one would expect that the observed peak intensity $I_E$ will increase with the square root of the concentration of that electrolyte ($C_E$, see Eq. (1.7)). At flow rates higher than that corresponding to the cone jet mode, the dependence on the concentration is lower than the 0.5 power [36]. Because ESI-MS is a very sensitive method, so that detection of electrolytes down to $10^{-8}$ M is easily feasible, one seldom works in practice with a single electrolyte system. The presence of electrolyte ions E leads to two concentration regimes for the analyte A:

(a) $C_A$ much higher than $C_E$. In that case, the $I_A$ is expected to increase with the square root (or slower) of $C_A$.

(b) $C_A$ much lower than $C_E$. In that case, $I_A$ is expected to increase with the first power of $C_A$ because now $I_A$ will depend on a statistical competition between $A^+$ and $E^+$ for being charges on the droplet surface.

To cover both regions, Tang and Kebarle [36] proposed Eq. (1.11a) for a two-component system in the positive ion mode. Equation (1.11a) predicts that when $C_E$ is much higher than $C_A$ and constant, the observed ion current $I_A$ will be proportional to $C_A$:

$$\text{Two components;} \quad I_{A^+} = pf \frac{k_A C_A}{k_A C_A + k_E C_E} I \tag{1.11a}$$

$$\text{Three components;} \quad I_{A^+} = pf \frac{k_A C_A}{k_A C_A + k_B C_B + k_E C_E} I \tag{1.11b}$$

$$\text{For } C_A = C_E; \quad I_A = \text{const} \times C_A \quad \text{const} = k_A I_E / k_E C_E \tag{1.11c}$$

Equation (1.11b) is for three components $A^+$, $B^+$, and $E^+$ with solution concentrations $C_A$, $C_B$, and $C_E$; $I$ is the total electrospray current leaving the spray capillary ($I$ can easily be measured, see Figure 1.1) and $p$ and $f$ are proportionality constants (see Ref. [36]). The sensitivity coefficients for $A^+$, $B^+$ and $E^+$ are $k_A$, $k_B$, and $k_E$ and depend on the specific chemical ability of the respective ion species to become part of the charge on the surface of the droplet and subsequently enter the gas phase. In the regime where $C_A \ll C_E$, Eq. (1.11a) reduces to Eq. (1.11c).

The experimental results [36] shown in Figure 1.7 give an example of a two-component system where the protonated morphine ($MorH^+$) is the analyte A, used at different concentrations, and the impurity ions $NH_4^+$ and $Na^+$, present at constant concentrations, are the electrolyte, E. The observed linear region of $MorH^+$ in the log–log plot used has a slope of unity at low concentrations ($10^{-8} - 10^{-5}$ M), which means that the $MorH^+$ ion is proportional to the morphine concentration. This region is suitable for quantitative determinations of analytes. At about $10^{-5}$ M the increase in the $MorH^+$ intensity slows down because the $MorH^+$ concentration used comes close to that of the impurity electrolytes. Above that region, where $MorH^+$ becomes the major electrolyte, the peak intensity of $MorH^+$ can increase only in proportion to the square root (or even a lower power) of the electrolyte concentration.

Experimental examination of a three-component system of two analytes (A and B) and the impurity (E) in order to determine the relative sensitivities $k_A$ and $k_B$ leads to an unexpected result (see Figure 1.8). In this experiment the concentrations of the two analytes tetrabutylammonium and cocaine (upper figure) or tetrabutylammonium and codeine (lower figure) are increased together such that $C_A = C_B$. The concentration ($C_E$) of the impurity is constant. It is easily shown using Eq. (1.11b) that when $C_A = C_B$ and $C_E$ is much larger than $C_A$ and $C_B$, the relationship $I_A/I_B = k_A/k_B$ holds. In the log–log plot used, the difference, $\log I_A - \log I_B$ should correspond to the difference $\log k_A - \log k_B = \log(k_A/k_B)$ and should be constant and in general not equal to zero. However, this is not the case (see Figure 1.8). The difference is constant only at high $C_A = C_B$ concentrations and becomes zero at low concentrations.
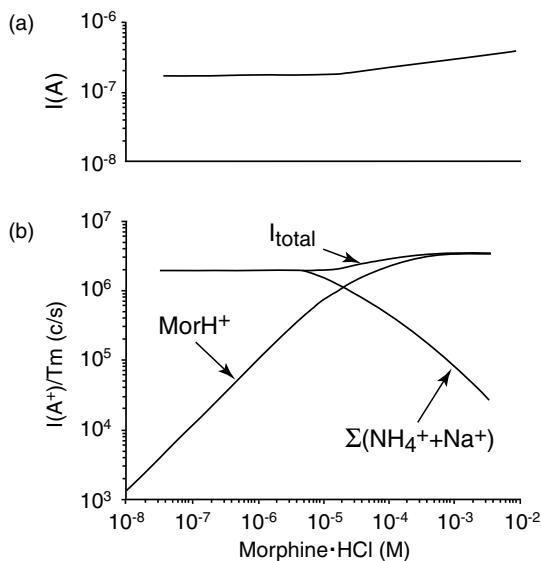
**Figure 1.7** (a) Total electrospray current (ampere) with increasing concentration of analyte morphine hydrochloride. Because of the presence of impurity ions ($Na^+$ and $NH_4^+$) at $10^{-5}$ M, $I_{total}$ remains constant up to the point where the analyte reaches concentrations above $10^{-5}$ M. (b) Analyte $MorH^+$ ion intensity (corrected for mass-dependent ion transmission, Tm, of quadrupole mass spectrometer used) is proportional to concentration of morphine hydrochloride up to the point where the morphine hydrochloride concentration approaches the concentration of impurity ions. Above that concentration, analyte ion increases much more slowly. (Reprinted from Ref. [36] with permission from the American Chemical Society.)

The tendency of $k_A/k_E$ to approach unity at low $C_A$ and $C_B$ indicates [36] that there is a *depletion* of the ion that has the higher sensitivity $k$. This is the tetrabutylammonium ion (A) in the present example. At $C_A = C_B \ll C_E \approx 10^{-5}$ M, the current $I$, the total charge $Q$ of the droplets, and the number of charged droplets are maintained by the presence of the electrolyte E, whose concentration is much higher. Under these conditions, species like $A^+$ and $B^+$ with large coefficients $k_A$ and $k_B$ find plenty of droplet surface to go to, and the ions evaporate rapidly even when present at very low concentrations. This results in a depletion of their concentration. The ion A of higher sensitivity is depleted more than B, and this leads to an apparent finding $k_A = k_B$.

Experimental determination of the coefficient ratios $k_A/k_B$ were performed [36] by working at high concentrations $C_A/C_B$ for a number of analytes in methanol. Under these conditions Eq. (1.11c) holds. It was found that the singly charged inorganic ions, $Na^+$, $K^+$, $Rb^+$, $Cs^+$, and $NH_4^+$ had low sensitivity coefficients, while analyte ions which were expected to be enriched on the droplet surface, that is, which were surface active, had high coefficients that increased with the surface activity of the ions. Thus, assuming that $k_{Cs} = 1$, the relative values $k_A$ for the ions were: $Cs^+ \approx 1$; $Et_4N^+ = 3$; $Pr_4N^+ = 5$; $Bu_4N^+ = 9$; $Pen_4N^+ = 16$; $HepNH_3^+ = 8$ (Et is ethyl,
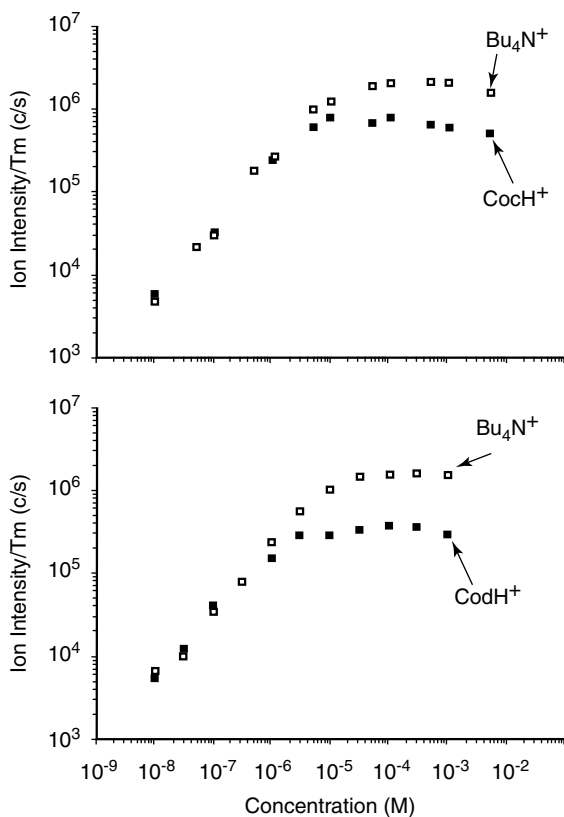
**Figure 1.8** Ion intensities (corrected for mass-dependent ion transmission, Tm, of quadrupole mass spectrometer used) for pairs of analytes at equal concentration in solution. The different ESI sensitivities of the analytes are observable only at high analyte concentrations (above $10^{-5}$ M). (Reprinted from Ref. [36] with permission from the American Chemical Society.)

Pr is *n*-propyl, Bu is *n*-butyl, Pen is *n*-pentyl, Hep is *n*-heptyl) see Table 1.1 in Tang, Kebarle [36]. The tetraalkyl ammonium salts and alkylammonium salts are known surfactants. It is notable that they can be used also as mass calibrants under nonaqueous, anaerobic conditions [37].

Assuming that IEM holds, ions from the droplet surface will leave the droplets and become gas-phase ions. In this case, the gas-phase ion sensitivity coefficient, $k_A$ for ions $A^+$ will depend on the relative surface population of the droplet surface, that is, on the surface activity of ions $A^+$ given by a surface activity equilibrium constant $K_{SA}$ and on the rate constant for ion evaporation. The rate constant for ion evaporation is also expected to increase with the surface activity of the ion, because surface active ions have low solvation energies (see Section 1.2.8). A third effect can also be expected. The droplets that lead to ion evaporation will, in general, be first, second or third generation progeny droplets, see Figure 1.5. Because the progeny droplets have

higher surface-to-volume ratios relative to the parent droplets, a large enrichment of the surface active ions is expected for the progeny droplets.

More recent work by Enke [38a], starting from somewhat different premises, led to further advances in predicting and understanding relative ion intensities. Instead of working with the ion currents $I$, $I_A$, a conversion to mole charge/liter was used. Thus the role of the total ion current $I$ was replaced with the molar concentration of the ionic charges $[Q]$. This can be done on the basis of Eq. (1.12);

$$[Q] = I/F\Gamma \tag{1.12}$$

where $[Q]$ is the $\mathrm{mol\,L^{-1}}$ electron charges; $I$ the total droplet current (TDC see Figure 1.1) in ampere (coulomb $\mathrm{s^{-1}}$); $F$ is Faraday's constant (96 485 coulomb) and $\Gamma$ is the flow rate in $\mathrm{L\,s^{-1}}$ through the spray capillary. The same type of relationship is also used in the conversion of the analyte currents $I_A$, $I_B$ and so on into molar concentrations of charges on the droplets due to the given ion species. Thus, $[A^+]_S$ is the molar concentration of charges on the surface of droplets due to $A^+$ species. The analyte $A^+$ was assumed to distribute itself between the interiors of the droplets with a concentration $[A^+]_I$ and as charge at the surface of the droplets $[A^+]_S$. It should be noted that while $[A^+]_I$ in $\mathrm{mol\,L^{-1}}$ is straightforward, $[A^+]_S$ as $\mathrm{mol\,L^{-1}}$ at the surface is not because expressing the surface as volume is unconventional. However, one could imagine that the ions (charges) at the surface are still interacting with a thin layer of solution below the surface, and this corresponds to a volume.

An equilibrium between $[A^+]_S$ and $[A^+]_I$ was assumed. The other electrolytes (E) were treated in the same way. Introduction of equations of charge balance and mass balance for each electrolyte led to an equation which predicts values for $[A^+]_S$, $[E^+]_S$ on the basis of the parameters $[Q]$, which is known (see Eq. (1.12)), the constants $K_A$, $K_E$ and the concentrations $C_A$, $C_E$. The assumption was made that $[A^+]_S$, $[E^+]_S$ will be converted to gas-phase ions and are therefore proportional with the same proportionality constant, $pf$ (see Eq. (1.11)) to the ion currents $I_A$, $I_E$. The equation of $[A^+]_S$, $[E^+]_S$ is of the same form as Eq. (1.11) in the high concentration range, but not in the low concentration range. By taking into account, via mass balance, the depletion of the concentration $C_A$, $C_E$ of the analytes with high coeffients $k_A = K_A$, $k_E = K_E$, the equation of Enke provides an excellent fit of the ion abundance curves, such as shown in Figure 1.8, over the full concentration range, preserving a constant $k_A/k_E$ ratio. Further development by Enke and coworkers has led to a most successful formalism. For other work by Enke and coworkers, dealing with the ESI mechanism and consequences for analytical work with ESI, see Ref. [38].

The preceding discussion deals with analytes that are charged, that is, ions in the solution used. When the analyte is not an ion in solution, charging of the analyte by ions that are present at the surface of the droplet can occur. It should be noted that at the surface the regime is very different from that in the bulk of the solvent. Suppose that the solution sprayed contains ammonium acetate ($NH_4Ac$) as additive and an organic analyte that has an unprotonated basic functional group because the basicity of that group is lower in solution than the basicity of $NH_3$. The ions at the surface of the droplets will be $NH_4^+$. Droplets that through evaporation and fission have reached the size where ion evaporation becomes possible could emit not only $NH_4^+$ but also

**Table 1.3** Some gas-phase basicities of bases B for reaction: $BH^+ = B + H^+$.

| Base | GP(B)$^a$ (kcal/mol) | Base | GP(B)$^a$ (kcal/mol) |
|---|---|---|---|
| $H_2O$ | 157.7 | $NH_3$ | 195.7 |
| $(H_2O)_2$ | 181.2 | $CH_3NH_2$ | 206.6 |
| $CH_3OH$ | 173.2 | $C_2H_5NH_2$ | 210.0 |
| $(CH_3OH)_2$ | 196.3 | $(CH_3)_2NH$ | 214.3 |
| $C_2H_5OH$ | 178.0 | $n$-$(C_3H_7)NH_2$ | 211.5 |
| $(CH_3)_2O$ | 179.0 | $N$-Methyl acetamide | 205.0 |
| $(C_2H_5)_2O$ | 182.7 | Pyridine | 214.8 |
| $CH_3CN$ | 191.0 | | |

$^a$GP(B) = Gas-Phase Basicity; GP(B)$^a$ = $\Delta G^o_{298}$ All values from NIST Database,
   http://webbook.nist.gov (Also used are Proton Affinities. They correspond to the $\Delta H^o$ value for the
   gas-phase reaction $BH^+ = B + H^+$).

protonated analytes because the basic group of the analyte might have a higher *gas-phase* basicity than that of $NH_3$. When the analyte is *at the surface*, the regime is gas-phase like and gas-phase basicites will count. There are large differences between *solution* and *gas-phase* basicities. For values of some gas-phase basicities, see Table 1.3. In the gas phase, in the absence of charge stabilizing solvent, basicities can increase with the size of the compound through dispersal of the charge in the analyte. This is the case for organic analytes where stabilization of the charge by charge dispersal can occur.

The discussion above also illustrates that under certain conditions, ESI may be 'blind' for analytes with low gas-phase basicity. This will be particularly the case when solutes other than the analyte are present at relatively high concentrations and have a higher gas-phase basicity than the analyte. In this case suitable charged groups will have to be introduced on the analyte (see for example Ref. [39]).

## 1.2.10
### Large Analyte Ions such as Dendrimers and Proteins are Most Probably Produced by the Charged Residue Model (CRM)

Although the first experiments of Dole used polystyrene, subsequent experiments by Fenn shifted attention to proteins and protein complexes that routinely can be produced in the gas phase by ESI. As a result, mechanistic studies have focused on these systems although other large synthetic supramolecular systems and polymers are expected to be transferred to the gas phase following the same mechanistic model. In the absence of sufficient data on synthetic macromolecular systems, subsequent sections will discuss mechanistic insights obtained using native proteins.

Native proteins are expected to remain folded when sprayed from neutral aqueous solutions. Under these conditions the folded (nondenatured) proteins lead to mass spectra consisting of a compact series of peaks that correspond to the molecular mass of the protein charged by a narrow range of $H^+$ ions when the positive ion mode is used. Thus, a small protein-like lysozyme (molecular mass

around 15 000 daltons) is observed to lead to three peaks due to three different charge states with $Z = 8$, 9 and 10. Obviously it is of special interest to understand why gas-phase proteins are multiply charged. Is the charge observed related to the protein charge in solution or are other factors involved which are due to the ESI mechanism?

An early study by R. D. Smith and coworkers [40] provided good evidence that proteins are produced via CRM. If CRM holds, one would expect that, when small charged droplets evaporate, there could be one protein but also more than one protein in such droplets, particularly so when high concentrations of the protein are used. Therefore, mass spectra should show the monomers, as originally present in solution, as well as multimers which are due to more than one protein being present in some of the final droplets. The authors observed a preponderance of multiply charged monomers and a rapidly decreasing series of low-intensity dimers, trimers, and higher multimers [40]. All of these results are consistent with CRM and a droplet evolution following a scheme of the type shown in Figure 1.5 [40].

In later work, Smith and coworkers [41a] found an interesting empirical correlation between the molecular mass, $M$, and the average charge, $Z_{\text{av}}$, see Eq. (1.13), of starburst dendrimers. Starburst dendrimers are multibranched alkylamine polymers that have relatively rigid structures and are close to spherical, that is, with shapes resembling those of globular proteins.

$$Z_{\text{av}} = aM^b \tag{1.13}$$

$Z_{\text{av}}$ is the observed average charge and $M$ the molecular mass of the dendrimer, while $a$ and $b$ are constants. The value $b = 0.53$ led to the best fit. An identical relationship was observed by Standing and coworkers [41b] for a large number of nondenatured proteins; a value between 0.52 and 0.55 was reported for $b$.

Independently Fernandez de la Mora [42] was able to show that the empirical relationship (Eq. (1.13)) holds and that this relationship can be derived on the basis of the charged residue mechanism. The plot shown in Figure 1.9 is based on data from the literature used by Fernandez de la Mora, but also includes the data of Standing *et al.* [41b]

The derivation of Fernandez de la Mora [42] was based on the following arguments. There was theoretical evidence that the evaporating charged droplets (which in the present context are assumed to contain one globular protein molecule) stay close to the Rayleigh limit. This is also supported by more recent experimental results [28] which involve charged evaporating water droplets of 5–35 μm diameter, as well as theoretical studies [43]. These show that the charge is approximately 95% of the Rayleigh limit when the droplets experience a Coulomb fission and approximately 75% of the Rayleigh limit immediately after the Coulomb fission. Thus, the droplets stay at all times within the limits of 95–75% of the Rayleigh limit, and both of these values are close to the Rayleigh limit. Fernandez de la Mora [42] reasoned that when the charged water droplet, containing one protein molecule, evaporates completely, the charges on the droplet will be transferred to the protein. He assumed also that the protein will be neutral when all the water is gone so that the charges on the surface of the droplet become the charge of the protein observed in the ESI mass
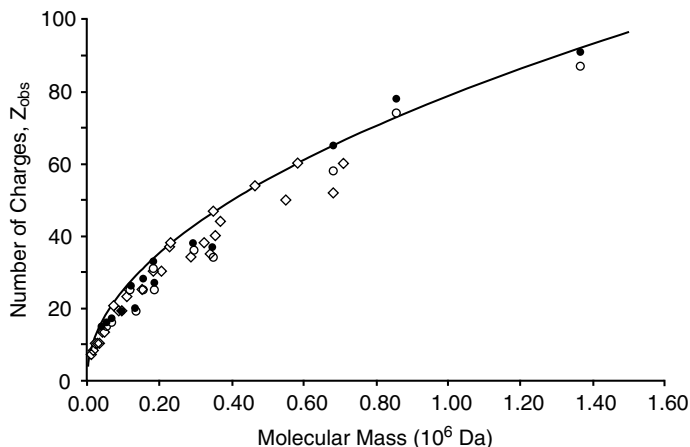
**Figure 1.9** Reproduction of a plot used by Fernandez de la Mora [42] and extended to include also data by Standing et al. [41b]. $Z_{obs}$ is the number of charges observed on proteins produced by ESI-MS under nondenaturing conditions, • highest charge, ○ lowest charge in mass spectrum (Fernandez de la Mora [42]). ◇ average $Z_{obs}$ (Standing et al. [41b]). Solid curve corresponds to charge $Z$ predicted by Eq. (1.14).

spectrum of the protein. Fernandez de la Mora further assumed that the nondenatured proteins have the same density φ as water. Evidence in support of that assumption, based on mobility measurements by Jarrold and Clemmer [44a,c] and Hodgins [44b], is given in Section 1.2.2 of Fernandez de la Mora [42], so that the radius $R$ of any *spherical* protein can be evaluated based on the molecular mass, without reference to the structure of the protein. The radius $R$ of the protein is evaluated with Eq. (1.14);

$$(4/3\pi R^3 \varphi)N_A = M \tag{1.14}$$

where φ is the density of the protein equal to that of water, $N_A$ is Avogadro's number, $R$ the radius of the protein, and $M$ the molecular mass of the protein.

The number of charges $Z$ on the protein is taken to be the same as the number of charges on a water droplet at the Rayleigh limit, with a radius equal to that of the protein. The number of charges $Z$ can be obtained by expressing the charge, $Q = Z \times e$, substituting it in the Rayleigh equation (Eq. (1.10)), and using the relationship between the molecular mass $M$ and the radius of the droplet (Eq. (1.14)). The result is given in Eq. (1.15a);

$$Z = 4(\pi\gamma\varepsilon_0/e^2 N_A \varphi)^{1/2} \times M^{1/2} \tag{1.15a}$$

$$Z = 0.078 \times M^{1/2} \tag{1.15b}$$

where $Z$ is the number of charges of the protein, γ the surface tension of water, $\varepsilon_o$ the electrical permittivity, $e$ the electron charge, $N_A$ is Avogadro number, φ the density of water, and $M$ the molecular mass of the protein. The constant 0.078

in Eq. (1.15b) gives the number of charges on a protein of molecular mass $M$ in megadaltons.

The solid curve in Figure 1.9 gives the predicted charge based on Eq. (1.15a). Good agreement with the experimental results is observed. Notable also is the predicted exponent of $M$ which is 0.5, while the exponent deduced from the experimental data [41a,b] is 0.53.

The agreement of Eq. (1.15) with the observed charges $Z$ can be considered as very strong evidence that globular proteins and protein complexes are produced by the charged residue mechanism. A recent compilation of data by Heck and coworkers [45] has shown that the square root dependence of the charge $Z$ on $M$ (see Eq. (1.15a)) also holds for protein complexes.

The experimental points in Figure 1.9 show considerable scatter and deviations from the theoretical curve. This is most likely because of the measurements being made in different laboratories or deviation from the assumed spherical form. Recent work by Katashov and Mohimen [46] (see Figure 1.10, in which all experimental points were obtained by the authors) and by Nesatyy and Suter [47] provide a very good fit. Kaltashov and Mohimen [46] have shown that in certain rare cases where the shape of the protein deviates strongly from spherical, the charge is determined not by the molecular mass but by the surface area of the protein. However, this finding [46] was based on a single protein (see point with considerable deviation in Figure 1.10), and the authors have not followed up with additional experiments.
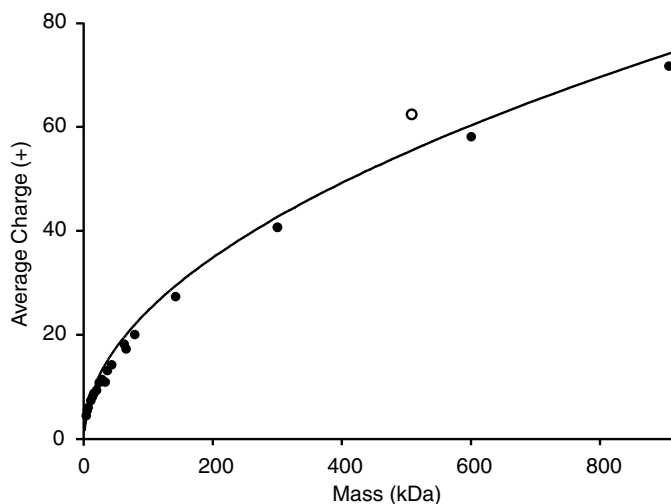


**Figure 1.10** Plot of average charge of proteins observed by Kaltashov and Mohimen [46] versus molecular mass of protein. The solid line curve gives average charge predicted by the Fernandez de la Mora equation, Eq. (1.14). A very good fit is observed except for one experimental point, for ferritin with a mass $\approx 510$ kDa which has a significantly higher charge $Z$. This protein is approximately spherical but has a cavity that increases its surface. (The Figure 1.10 plot was kindly provided to the authors by Dr. Justin Benesh.)

Fernandez de la Mora [42] did not consider the actual chemical reactions by which the charging of the protein occurs. These reactions will depend on what additives were present in the solution. Thus, in the presence of 1% of acetic acid in the solution, the charges at the surface of the droplets will be $H_3O^+$ ions. Charging of the protein will occur by proton transfer from $H_3O^+$ to functional groups on the surface of the protein that have a higher gas-phase basicity than $H_2O$. The *gas*-phase basicities are relevant because the solvent will essentially have disappeared. There are plenty of functional groups on the protein that have gas-phase basicities that are higher than that of $H_2O$. These could be basic residues or amide groups of the peptide backbone at the surface of the protein. Gas-phase basicities of several representative compounds are given in Table 1.3.

In summary, the Charged Residue Mechanism has allowed quantitative predictions of the protein charge state in the gas phase and is well supported for large proteins of widely varying mass. It is likely that it will be important also for the analysis of larger supramolecular and polymeric systems.

### 1.2.11
### Nanospray and Insights into Fundamentals of Electro and Nanospray

Nanospray was developed by Wilm and Mann [48, 49]. Their primary interest was an electrospray device that requires much smaller quantities of analyte. Such a device would be particularly important in situations where only very small amounts of the analyte are available. Most of the analyte is wasted using ESI. The large diameter of the spray tip produces large droplets whose evolution to small droplets requires the presence of a large distance between the spray tip and the sampling orifice or capillary (see Figures 1.1 and 1.2a). As a result, only a small fraction of the generated gas-phase ions enter the sampling orifice/capillary.

With nanospray, the spray tip has a much smaller diameter. Also, for the by far most often used nonviscous solutions, the flow is not a forced flow due to a driven syringe as used in ESI (see Figure 1.2a). Instead, the entrance end of the spray capillary is left open and a 'self-flow' results, which is due to the pull of the applied electric field on the solution at the capillary tip (see Section 1.2.2). This self-flow is controlled by the diameter of the tip of the spray capillary.

In their first effort [48], using what was essentially an electrospray source, Wilm and Mann developed an equation for the radius of the zone at the tip of the Taylor cone from which the charged droplets are ejected. This radius is related to the resulting droplets' radii, see Figure 1.3a. It was found that the radius depends on the 2/3 power of the flow rate. To minimize the radius of the zone, a modified electrospray ion source with a smaller orifice was developed which led to a 'microspray' version of ESI. Further development [49] using capillary orifices as small as 1–2 μm diameter, led to nanospray. Such small orifices could be obtained by pulling small diameter borosilicate capillaries with a microcapillary puller. About 1 μL of solvent is loaded directly into the wide entrance end of the capillary. The droplets produced had a volume that was close to 1000 times smaller than the volume of droplets obtained with conventional ESI. Such small droplets will

evaporate very rapidly, so that the capillary tip can be placed very close to the sampling orifice that leads to the mass spectrometer, thereby minimizing sample loss and allowing efficient use of a large fraction of the solution subjected to MS analysis. Therefore, even though the amount of analyte sample used is 10–100 times smaller than that used with ESI, the observed mass spectrum peak intensities are equal if not larger than those in conventional ESI. Nanoelectrospray has proven to be of enormous importance for the analysis of biochemical and biopharmaceutical samples. So far, the use of nanoelectrospray in physical organic or organometallic chemistry has not been reported and remains to be explored (see Section 1.2.12.2).

Nanoelectrospray is also important to research on the fundamentals of electrospray and nanospray. Karas and coworkers [50–52] have been major contributors to this research.

Experimentally it was found that the mass spectra of analytes showed much less dependence on background electrolytes (such as sodium) when nanospray was used for the electrostatic dispersion. Gas-phase ions are produced from charged droplets only when the droplets are very small. This holds both for IEM and CRM. Therefore, if one starts with relatively small initial droplets as generated with nanospray, much less solvent evaporation will be required to reach the final droplet size required for the generation of gas-phase ions. Therefore, in the presence of impurities such as sodium salts the concentration increase of the salt will be much smaller with nanospray.

In an extension and expansion of the above work [50], Schmidt *et al.* [51] studied the effect of different solution flow rates on the analyte signal. A series of analytes was chosen that have decreasing surface activities. The authors found that the ion abundance of the analyte with low surface activity was suppressed at higher 'ESI-like' flow rates, while at the lowest flow rates this suppression disappeared. At high flow rates, the charged droplets emitted from the spray tip are much larger and require extended evaporation and successive fission events before the final droplets are reached. Droplet evaporation as well as each fission increase the surface-to-volume ratio of the droplets. As a result, surface-active analytes will preferentially enter the progeny droplets, leading to a high ion abundance for the surface-active analytes. Considering nanospray and the corresponding low flow rate, very small initial droplets will be obtained and the evolution to the final droplet will be very short. In the extreme, there would be no such evolution and this would lead to minimal discrimination against analytes that are not surface active.

Another well-documented work by Chernushevich, Bahr, and Karas [52] deals with a disadvantage of nanospray relative to conventional electrospray. Using nanospray some analytes were found to appear with delays of tens of minutes; a few analytes were not detected at all. No such suppression was found with ESI. The effect was found to be related to cation exchange on glass surfaces. Glass surfaces are known to be negatively charged and are thus expected to retain positive ions. The surface ion-exchange problem in nanospray could simply be avoided by using pure silica capillaries.
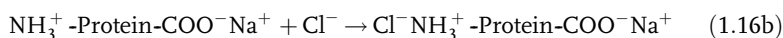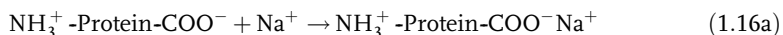
### 1.2.12
### Consequences of the Increase in Concentration Caused by Extensive Evaporation of Solvent in ESI Process. Promotion of Bimolecular Reactions Involving Analyte Ions

As discussed in Section 1.2.7, the formation of the final charged droplets that lead to gas-phase ions is associated with a very large loss of solvent by evaporation. This leads to a large increase in the concentration of the solutes present in the electrosprayed solution. Such a large increase in concentration will promote bimolecular reactions, and these will have an effect on the observed mass spectrum. We will consider two examples. In the first example bimolecular reactions are shown to take place on native proteins, indicating various levels of protein *surface* gas-phase chemistry. In the second example, a comparison of biochemical and physical organic applications of ESMS to the determination of equilibrium constants indicates the limitations on such measurements imposed by the electrospray mechanism.

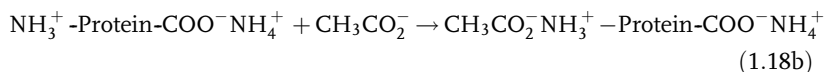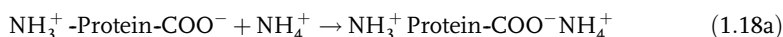#### 1.2.12.1 Positive-Negative Ion-Pairing Reactions Involving Impurities such as $Na^+$
Sodium ions are a common impurity in solvents used for ESI. Analyte samples (especially proteins) are often contaminated by sodium ions in the production process, while sample solution storage in glass vessels also contributes to the sodium contamination. The extensive evaporation of solvent in the ESI process promotes solution ion-pairing reactions. When the analyte is a protein, ion-pairing reactions will involve $Na^+$ and the ionized acid residues of the protein, see Eq. (1.16a). Similarly, impurity anions such as $Cl^-$ will ion pair with ionized basic residues of the protein (see Eq. (1.16b)).

$$NH_3^+\text{-Protein-COO}^- + Na^+ \rightarrow NH_3^+\text{-Protein-COO}^-Na^+ \tag{1.16a}$$

$$NH_3^+\text{-Protein-COO}^-Na^+ + Cl^- \rightarrow Cl^-NH_3^+\text{-Protein-COO}^-Na^+ \tag{1.16b}$$

The occurrence of these ion pairing reactions was demonstrated by Verkerk and Kebarle [53]. In the collisional activation stage of the ESI-MS dissociation occurs following Eq. (1.17):

$$Cl^-NH_3^+\text{-Protein-COO}^-Na^+ \rightarrow H_2N\text{-Protein-COO}^-Na^+ + HCl \tag{1.17}$$

Thus the $Na^+$ adduct remains while the $Cl^-$ pulls off a proton from the basic residue of the protein. In general there are at least several acidic residues at the surface of proteins and the addition of sodium to most of these leads to mass spectra that are difficult to interpret. The authors [53] also demonstrated that one can prevent the undesirable sodium addition by adding a millimolar concentration of ammonium acetate to the solution. Because the concentration of ammonium acetate is much higher than that of the impurity ions, ion pairing of $NH_4^+$ with the acidic residue $CH_3CH_2CO_2^-$ and ion pairing of $CH_3CO_2^-$ with the basic residue occur as shown below:

$$NH_3^+\text{-Protein-COO}^- + NH_4^+ \rightarrow NH_3^+ \text{Protein-COO}^-NH_4^+ \tag{1.18a}$$

$$NH_3^+\text{-Protein-COO}^-NH_4^+ + CH_3CO_2^- \rightarrow CH_3CO_2^-NH_3^+ -\text{Protein-COO}^-NH_4^+ \tag{1.18b}$$

This result may seem an undesirable change. However in the clean up stages of the ESI-MS these ion pairs are unstable; intramolecular proton transfer occurs followed by dissociation resulting in the products (Eq. (1.19)):

$$CH_3CO_2^- NH_3^+ \text{-Protein-}COO^- NH_4^+ \rightarrow NH_2\text{-Protein-}COOH + NH_3 + CH_3CO_2H$$

$$(1.19)$$
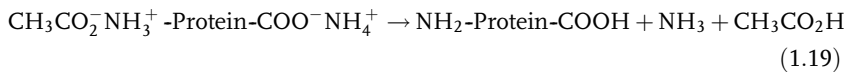
Because the ammonium acetate concentration is much higher than that of impurities such as sodium ions, reactions, such as Eq. (1.16) are prevented. A clean mass spectrum results and the protein appears at the right mass. In ESI-MS practice, ammonium acetate is routinely used as an additive and the assumption is made that its purpose is to act as a buffer. The above findings [53] demonstrate that the popularity of ammonium acetate may not due to its action as a buffer but on its ability to lead to clean mass spectra.

### 1.2.12.2 Determination of Equilibrium Constants in Solution via ESI-MS

Electrospray mass spectrometry may appear a very attractive technique for the determination of the equilibrium constant of a reaction occurring in solution because of the soft nature of ESI, the simultaneous determination of the relative ion abundance of the reactants participating in the equilibrium, the high sensitivity, and the low sample consumption.

The determinations of equilibrium constants using ESI-MS can be divided into two categories: (a) equilibria of small positive ions and ligands (such as crown ethers), so that the gas-phase ion creation involves IEM, and (b) equilibria of macro ions (such as proteins) and ligands (which may or may not be large organic molecules) so that gas-phase ion creation involves CRM.

However, uncritical application of ESI-MS can lead to erroneous results due to the complexity of the electrospray process. First of all, ESI-MS spectra are sensitive to instrumental parameters, and these therefore must be chosen in such a way as to minimize such effects. Secondly, during the charged droplets evaporation, the concentration and pH of the sampled solution changes. If the equilibrium rate constants are high enough, the observed ligand-substrate ratio may reflect the concentration changes experienced during the evaporation/ionization step and thus lead to erroneous determinations of the equilibrium constant in solution.

Consider the general reaction, Eq. (1.20a), where P is a ligand and S is a substrate, in a reaction that has reached equilibrium in the solution used. The equilibrium constant $K_{AS}$ is given by Eq. (1.20b) where [P], [S] and [PS] are the concentrations at equilibrium.

$$P + S = PS \tag{1.20a}$$

$$K_{AS} = [PS]/[P] \times [S] = I_{PS}/I_P \times I_S \tag{1.20b}$$

Sampling the solution with ESI, the concentrations can be replaced with the ESI-MS observed peak intensities $I_P$, $I_S$ and $I_{PS}$ assuming that the individual sensitivity coefficients are equal to one. However this cannot be expected, and different strategies have been proposed to deal with this, see reference [54].

Thus, one can repeat the experiment at several, gradually increasing, concentrations of S and examine whether the association constant, evaluated with Eq. (1.20b), remains constant. This procedure is called the 'Titration Method' and is generally used in ESI-MS determinations of the equilibrium constant. When the differences in molecular mass of S, P or PS are large, erroneous results may be obtained due to $m/z$-dependent transmission differences of the MS analyzer. While less of a problem for small metal (S)-ligand-(P) interactions, for proteins (P) of very large mass and substrate (S) of much smaller mass it is advantageous to use only the ratio $I_{PS}/I_P$. Zenobi and coworkers [55] have provided an equation for the determination of $K_{AS}$ in which only the ratio $I_{PS}/I_P$ is used.

From the standpoint of the mechanism of ESI, an agreement of the $K_{AS}$ values determined via ESI-MS with values obtained with conventional in-solution methods may appear surprising. One could expect that the very large increase in the concentration of the solutes in the charged droplets due to evaporation of the solvent in the droplet evolution will lead to an apparent $K_{AS}$ that is much too high. However, this equilibrium shift need not occur if rates of the forward and reverse reactions leading to the equilibrium are slow compared to the time of droplet evaporation.

Peschke *et al.* [33] evaluated an approximate droplet history scheme for water droplets produced by nanoelectrospray. The early part of this scheme is shown in Figure 1.5, Section 1.2.7. Because the initial droplets produced by nanospray have a small diameter ($< 1\,\mu m$), their evaporation is very fast, so that they reach the Rayleigh instability condition in just a few $\mu s$. It could also be established that the first generation progeny droplets will be the major source of analyte ions [33].

Assuming even the fastest possible reaction rates, that is, the diffusion limit rates for the forward reaction $P + S = PS$, it could be shown that the total droplet evaporation time can be too short for the equilibrium (Eq. 1.20b) to shift in response to the increasing concentration due to solvent evaporation. The rate constant at the diffusion limit decreases with an increase in the substrate size. Substrates of medium size such as erythrohydroxy aspartate, adenosine di- and tri-phosphate, with diffusion-limited rate constants $k$ from $10^6$ to $10^7\,M^{-1}\,s^{-1}$, are too slow to cause an equilibrium shift that will lead to a significant error in the equilibrium constant ($K_{AS}$) determination via ESI-MS. Thus, an equilibrium shift for substrates that are not too small is not expected using nanospray. This is in contrast to electrospray, where droplet evaporation takes place in the millisecond range [36]. It is noteworthy that, as far as we are aware, electrospray is the method most used for equilibrium measurements of small metal-ligand systems, while our analysis indicates that the use of nanospray may be less error-prone. For a thorough review on small metal-ligand systems, see Ref. [54]. More recent investigations on small systems are reported in work by Zenobi and coworkers [56].

Because large complexes are most probably transferred to the gas phase via CRM, another question must also be examined. Considering a protein-substrate complex, and assuming close to equal concentrations of protein (P) and substrate (S), an evaluation [33] shows that, for an initial concentration of $10\,\mu M$, in most cases there will be one protein and one substrate molecule in the average first generation progeny droplet that has evaporated down to the size of the protein. In that case,

protein and substrate will form a nonspecific complex because the substrate makes a random encounter with the protein and has 'no time' to find the site of specific strong bonding. Since the mass of the nonspecific complex is the same as that of the specific complex, the observed peak intensity ($I_{SP}$) will lead to an apparent $K_{AS}$ that is too high. If however the nonspecific complex is weakly bound, the nonspecific contribution in the measured $K_{AS}$ could be minimized because of dissociation in the clean-up stages of the electrospray process. This *a priori* assumption about weakly bound nonspecific complexes being decomposed in the clean-up stage may not predict the correct outcome in all cases. It neglects to consider the strong ion-neutral bonding in the gas phase and the fact that the protein will be multiply charged. Strong hydrogen bonds can form between charged (protonated) sites of the protein and functional groups of the substrate such as $-OH$ and $-NH_2$ groups. A recent study by Wang, Kitova, and Klassen [57] exactly described such effects for protein (P)-carbohydrate (S) complexes. In this study, accidental PS and SPS complexes were observed in the gas phase and the nonspecific bond was found to be stronger than the specific bond. This suggested that the nonspecific S-P bond was to a protonated site of the charged protein [57]. These results are not surprising; proton-bridged dimers have long been known to form very strong bonds in the gas phase [58]. Further important examples of the use of ESI-MS in the study of large noncovalent complexes are provided in Ref. [59].

The above examples provide a good illustration of the fact that an understanding of the ESI-MS mechanisms is necessary for the correct interpretation of results obtained with ESI-MS.

## References

**1** (a) Bakhtiar, R. and Hop, C.E.C.A. (1999) Unravelling seemingly complex chemistry of reactions using electrospray ionization mass spectrometry. *J. Phys. Org. Chem.*, **12**, 511–527; (b) Traeger, J.C. (2000) Electrospray mass spectrometry of organometallic compounds. *Int. J. Mass Spectrom.*, **200**, 387–401; (c) Chen, P. (2003) Electrospray ionization tandem mass spectrometry in high throughput screening of homogeneous catalysis. *Angew. Chem. Int. Ed.*, **42**, 2832–2847; (d) Griep-Raming, J., Meyer, S., Bruhn, T., and Metzger, J.O. (2002) investigation of reactive intermediates of chemical reactions in solution by electrospray ionization mass spectrometry: radical chain reactions. *Angew. Chem. Int. Ed.*, **41**, 2738–2742; (e) Santos, L.S., Knaack, L., and Metzger, J.O. (2005) Investigations of Chemical Reactions in Solution using API MS. *Inter. J. Mass Spectrom.*, **246**, 84–1004.

**2** Fenn, J.B. Electrospray Wings for Molecular Elephants. Nobel Lecture available on web: http://nobelprize.org/nobel_prizes/chemistry/laureates/2002/fenn-lecture.pdf.

**3** (a) Chapman, S. (1937) Carrier mobility spectra of spray electrified liquids. *Phys. Rev.*, **52**, 184–190; (b) Chapman, S. (1938) Carrier mobility spectra of liquids electrified by bubbling. *Phys. Rev.*, **54**, 520–527.

**4** Dole, M. (1989) *My Life in the Golden Age of America*, Vantage Press, New York, p. 69; (b) Dole, M., Mack, L.L., Hines, R.L.,

Mobley, R.C., Ferguson, L.D., and Alice, M.B. (1968) Molecular beams of macroions. *J. Chem. Phys.*, **49**, 2240–2249.

5 (a) Yamashita, M. and Fenn, J.B. (1984) Electrospray ion source. Another variation of the free-jet theme. *J. Phys. Chem.*, **88**, 4451–4459; (b) Yamashita, M. and Fenn, J.B. (1984) Negative ion production with the electrospray ion source. *J. Phys. Chem.*, **88**, 4672–4675.

6 Whitehouse, C.M., Dreyer, R.N., Yamashita, M., and Fenn, J.B. (1985) Electrospray interface for liquid chromatographs and mass spectrometers. *Anal. Chem.*, **57**, 675–679.

7 Smith, R.D., Loo, J.L., Ogorzalek-Loo, R.R., Busman, M., and Udseth, H.R. (1991) Principles and practice of electrospray ionization mass spectrometry for large peptides and proteins. *Mass Spectrom. Reviews*, **10**, 359–451.

8 Electrospray: theory and applications. Special Issue *J. Aerosol Sci.*, **25**, (1994) 1005–1252.

9 (a) Loeb, L., Kip, A.F., Hudson, G.G., and Bennet, W.H. (1941) Pulses in negative point-to-plane corona. *Phys. Rev.*, **60**, 714–722; (b) Pfeifer, R.J. and Hendricks, C.D. (1968) Parametric studies of electrohydrodynamic spraying. *AIAAJ*, **6**, 496–502.

10 (a) Grace, J.M. and Marijnissen, J.C.M. (1994) A review of liquid atomization by electrical means. *J. Aerosol Sci.*, **25**, 1005–1019; (b) Szabo, P.T. and Kele, Z. (2001) Electrospray mass spectrometry of hydrophobic compounds using dimethyl sulfoxide and dimethylformamide as solvents. *Rapid Comm. Mass Spectrom.*, **15**, 2415–2419; (c) Henderson, M.A. and McIndoe, J.S. (2006) Ionic liquids enable electrospray ionisation mass spectrometry in hexane. *Chem. Commun.*, 2872–2874.

11 Taylor, G.I. (1965) The stability of horizontal fluid interface in a vertical electric field. *J. Fluid. Mech.*, **2**, 1–15.

12 Fernandez de la Mora, J. (2007) The fluid dynamics of Taylor cones. *J. Ann. Rev. Fluid. Mech.*, **39**, 217–243.

13 (a) Cloupeau, M. and Prunet-Foch, B. (1994) Electrohydrodynamic spraying functioning modes: a critical review. *J. Aerosol Sci.*, **25**, 1021–1036; (b) Cloupeau, M. (1994) Recipes for use of EHD spraying in cone-jet mode and notes on corona discharge. *J. Aerosol Sci.*, **25**, 1143–1157; (c) Cloupeau, M. and Prunet-Foch, B. (1989) Recipes for use of EHD spraying of liquids in cone-jet mode. *J. Aerosol Sci.*, **22**, 165–184.

14 Tang, K. and Gomez, A. (1994) On the structure of an electrospray of monodisperse droplets. *Phys. Fluids*, **6**, 2317–2322; (b) Tang, K. and Gomez, A. (1994) Generation by electrospray of monodisperse water droplets for targeted drug delivery by inhalation. *J. Aerosol Sci.*, **25**, 1237–1249; (c) Tang, K. and Gomez, A. (1995) Generation of monodisperse water droplets from electrosprays in a corona-assisted cone-jet mode. *J. Colloid Sci.*, **175**, 326–332; (d) Tang, K. and Gomez, A. (1996) Monodisperse electrosprays of low electric conductivity liquids in the cone-jet mode. *J. Colloid Sci.*, **184**, 500–511.

15 Marginean, I., Parvin, L., Heffernan, L., and Vertes, A. (2004) Flexing the electrified meniscus: the birth of a jet in electrosprays. *Anal. Chem.*, **76**, 4202–4207.

16 Blades, A.T., Ikonomou, M.G., and Kebarle, P. (1991) Mechanism of electrospray mass spectrometry. Electrospray as an electrolysis cell. *Anal. Chem.*, **63**, 2109–2114.

17 (a) Van Berkel, G.J. (2000) insights into analyte electrolysis in an electrospray emitter from chronopotentiometry experiments and mass transport calculations. *J. Am. Soc. Mass Spectrom.*, **11**, 951–960; (b) Van Berkel, G.J., Zhou, F., and Aronson, J.T. (1997) Changes in bulk solution pH caused by the inherent controlled-current electrolytic process of an electrospray ion source. *Intern. J. Mass Spectrom. Ion Process.*, **162**, 55–62; (c) Van Berkel, G.J. and Zhou, F. (1996) Observation of gas-phase molecular dications formed from neutral organics in

solution via the controlled-current electrolytic process inherent to electrospray. *J. Am. Soc. Mass Spectrom.*, **7**, 157–162; (d) Zhou, F., Van Berkel, G.J., and Donovan, B.T. (1994) Electron-transfer reactions of fluorofullerene $C_{60}F_{48}$. *J. Am. Chem. Soc.*, **116**, 5485–5486; (e) Van Berkel, G.J., McLuckey, S.A., and Glish, G.L. (1991) Performing ions in solution via charge-transfer complexation for analysis by electrospray ionization mass spectrometry. *Anal. Chem.*, **63**, 2064–2068.

18  Moini, M., Cao, P., and Bard, A.J. (1999) Hydroquinone as a buffer additive for suppression of bubbles formed b electro-chemical oxidation of the CE buffer at the outlet electrode in capillary electrophore-sis/electrospray ionization-mass spectro-metry. *Anal. Chem.*, **71**, 1658–1661.

19  Smith, D.P.H. (1986) The electrohydrodynamic atomization of liquids. *IEEE Trans. Ind. Appl.*, **22**, 527–535.

20  Ikonomou, M.G., Blades, A.T., and Kebarle, P. (1991) Electrospray mass spectrometry of methanol and water solutions. Suppression of electric discharge with $SF_6$ gas. *J. Am. Soc. Mass Spectrom.*, **2**, 497–505.

21  Wampler, F.W., Blades, A.T., and Kebarle, P. (1993) Negative ion electrospray mass spectrometry of nucleotides: ionization from water solution with $SF_6$ discharge suppression. *J. Am. Soc. Mass Spectrom.*, **4**, 289–295.

22  (a) Jaworek, A., Czech, T., Rajch, E., and Lackowksi, M. (2005) Spectroscopic studies of electric discharges in electrospraying. *J. Electrost.*, **63**, 635–641; (b) Jaworek, A. and Krupa, A. (1997) Studies of corona discharge in EHD spraying. *J. Electrost.*, **40/41**, 173–178.

23  Fernandez-de la Mora, J. and Locertales, I.G. (1994) The current emitted by highly conducting taylor cones. *J. Fluid. Mech.*, **260**, 155–184.

24  Cherney, L.T. (1999) Structure of the taylor cone jets: limit of low flow rates. *J. Fluid. Mech.*, **378**, 167–196.

25  Chen, D.R. and Pui, D.Y.H. (1997) Experimental investigations of scaling laws for electrospray: dielectric constant effect. *Aerosol Sci. Technology*, **27**, 367–380.

26  Rayleigh, L. (1882) On the equilibrium of liquid conducting masses charged with electricity. *Phil. Mag. Ser. 5*, **14**, 184–186.

27  Gomez, A. and Tang, K. (1994) Charge and fission of droplets in electrostatic sprays. *Phys. Fluids.*, **6**, 404–414.

28  (a) Smith, J.N., Flagan, R.C., and Beauchamp, J.L. (2002) Droplet evaporation and discharge dynamics in electrospray ionization. *J. Phys. Chem. A.*, **106**, 9957–9967; (b) Grimm, R.L. and Beauchamp, J.L. (2002) Evaporation and discharge dynamics of highly charged droplets of heptane, octane and p-xylene generated by electrospray ionization. *Anal. Chem.*, **74**, 6291–6297.

29  Taflin, D.C., Ward, T.L., and Davis, E.J. (1989) Electrified droplet fission and the Rayleigh limit. *Langmuir*, **5**, 376–384.

30  Richardson, C.B., Pigg, A.L., and Hightower, R.L. (1989) On the stability limit of charged droplets. *Proc. Roy. Soc. A.*, **422**, 319–328.

31  Schweitzer, J.W. and Hanson, D.N. (1971) Stability limit of charged drops. *J. Colloid Interface Sci.*, **35**, 417–423; (b) Duft, D., Achtzehn, T., Muller, R., Huber, B.A., and Leisner, T. (2003) Rayleigh jets from levitated microdroplets. *Nature*, **421**, 128.

32  (a) Loscertales, I.G. and Fernandez de la Mora, J. (1995) Experiments on the kinetics of field evaporation of small ions from droplets. *J. Chem. Phys.*, **103**, 5041–5060; (b) Gamero-Castano, M. and Fernadez de la Mora, J. (2000) Kinetics of small ion evaporation from the charge and mass distribution of multiply charged clusters in electrosprays. *J. Mass Spectrom.*, **35**, 790–803; (c) Gamero-Castano, M. and Fernandez de la Mora, J. (2000) Direct measurement of ion evaporation kinetics from electrified liquid surfaces. *J. Chem. Phys.*, **113**, 815–832.

33  Peschke, M., Verkerk, U.H., and Kebarle, P. (2004) Features of the ESI mechanism

that affect the observation of multiply charged noncovalent complexes and the determination of the association constant by the titration method. *J. Am. Soc. Mass Spectrom.*, **15**, 1424–1434.

34 (a) Iribarne, J.V. and Thomson, B.A. (1976) On the evaporation of small ions from charged droplets. *J. Chem. Phys.*, **64**, 2287–2294; (b) Thomson, B.A. and Iribarne, J.V. (1979) Field induced ion evaporation from liquid surfaces at atmospheric pressure. *J. Phys. Chem.*, **71**, 4451–4463.

35 Znamenskiy, V., Marginean, I., and Vertes, A. (2003) Solvated ion evaporation from charged water nanodroplets. *J. Phys. Chem. A.*, **107**, 7406–7412.

36 Tang, L. and Kebarle, P. (1993) Dependence of the ion intensity in electrospray mass spectrometry on the concentration of the analytes in the electrosprayed solution. *Anal. Chem.*, **65**, 3654–3668.

37 Lubben, A.T., McIndoe, J.S., and Weller, A.S. (2008) Coupling an electrospray ionization mass spectrometer with a glovebox: a straightforward, powerful, and convenient combination for analysis of air-sensitive organometallics. *Organometallics*, **27**, 3303–3306.

38 (a) Enke, C.G. (1997) A predictive model for matrix and analyte effects in the electrospray ionization of singly-charged ionic analytes. *Anal. Chem.*, **69**, 4885–4893; (b) Cech, N.B. and Enke, C.G. (2006) Electrospray ionization mass spectrometry: how and when it works, in *Encyclopedia of Mass Spectrometry*, vol. 8 (eds M.L. Gross and R. Caprioli), Pergamon, New York, pp. 171–180; (c) Enke, C.G. (1997) A predictive model for matrix and analyte effects in electrospray ionization of singly-charged ionic analytes. *Anal. Chem.*, **69**, 4885–4893; (d) Cech, N.B. and Enke, C.G. (2001) The effect of affinity for charged droplet surfaces on the fraction of analyte charged in the electrospray process. *Anal. Chem.*, **73**, 4632–4639; (e) Amad, M.H., Cech,

N.B., Jackson, G.S., and Enke, C.G. (2000) Importance of gas-phase proton affinities in determining the electrospray ionization response for analytes and solvents. *J. Mass Spectrom.*, **35**, 784–789.

39 Chisholm, D.M. and McIndoe, J.S. (2008) Charged ligands for catalyst immobilisation and analysis. *Dalton Trans.*, 3933–3945.

40 Winger, B.A., Light-Wahl, K.J., Ogorzalek-Loo, R.R., Udseth, H.R., and Smith, R.D. (1993) Observations and implications of high mass-to-charge ratio ions from electrospray ionization mass spectrometery. *J. Am. Soc. Mass. Spectrom.*, **4**, 536–545.

41 (a) Tolic, R.P., Anderson, G.A., Smith, R.D., Brothers, H.M., Spindler, R., and Tomalia, D.A. (1997) Electrospray ionization fourier transform ion cyclotron resonance mass spectrometric characterization of high molecular mass starburst (TM) dendrimers. *Int. J. Mass Spectrom. Ion Proc.*, **165/166**, 405–418; (b) Chernuschevich, I.V., Ens, W., and Standing, K.G. (1998) *New Methods for the Study of Biomolecular Complexes* (eds W. Ens, K.G. Standing, and I.V. Chernuschevich), Kluwer Academic Publishers, Dordrecht, Boston, London, pp. 101–117.

42 Fernandez de la Mora, J. (2000) Electrospray ionization of large multiply charged species proceeds via Dole's charged residue mechanism. *Anal. Chim. Acta*, **406**, 93–104.

43 Shrimpton, J.S. (2005) Dielectric charged drop break-up at sub-rayleigh limit conditions. *IEEE Trans. Dielec. Elec. Ins.*, **12**, 573–578.

44 (a) Valentine, S.J., Anderson, J.G., Ellington, D.E., and Clemmer, D.E. (1997) Disulfide intact and reduced lysozyme in the gas-phase: conformations and pathways of folding and unfolding. *J. Phys. Chem B*, **101**, 3891–3900; (b) Hudgins, R.R. (1997) High resolution ion mobility measurements for gas-phase conformations. *Int. J. Mass Spectrom.*, **165**,

497–507; (c) Shelimov, K.B., Clemmer, D.E., Hudgins, R.R., and Jarrold, M. (1997) Protein structure *in vacuo*: gas-phase conformations of BPTI and cytochrome C. *J. Am. Chem. Soc.*, **119**, 2240–2248.

**45** Heck, A.J.R. and van den Heuvel, R.H.H. (2004) Investigation of intact protein complexes by mass spectrometry. *Mass Spectrom. Rev.*, **23**, 368–389.

**46** Kaltashov, I.A. and Mohimen, A. (2005) Estimates of protein areas in solution by electrospray ionization mass spectrometry. *Anal. Chem.*, **77**, 5370–5379.

**47** Nesatty, V.J. and Suter, M.J.F. (2004) On the conformation-dependent neutralization theory and charging of individual proteins and their non-covalent complexes in the gas phase. *J. Mass Spectrom.*, **39**, 93–97.

**48** Wilm, M. and Mann, M. (1994) Electrospray and Taylor-cone theory, Dole's beam of macromolecules at last? *Int. J. Mass Spectrom. Ion Proc.*, **136**, 167–180.

**49** Wilm, M. and Mann, M. (1996) Analytical properties of the nanoelectrospray ion source. *Anal. Chem.*, **68**, 1–8.

**50** Juraschek, R., Dulks, T., and Karas, M. (1999) Nanoelectrospray - more than just a minimized-flow electrospray ion source. *J. Am. Soc. Mass Spectrom.*, **10**, 300–308.

**51** Schmidt, A., Karas, M., and Dulks, T. (2003) Effect of different solution flow rates on analyte signals in nano-ESI-MS, or: when does ESI turn into nano-ESI. *J. Am. Soc. Mass Spectrom.*, **14**, 492–500.

**52** Chernushevich, I.V., Bahr, U., and Karas, M. (2004) Nanospray taxation and how to avoid it. *Rapid Commun. Mass Spectrom.*, **18**, 2479–2485.

**53** Verkerk, U.H. and Kebarle, P. (2005) Ion-ion and ion-molecule reactions at the surface of proteins produced by nanospray. Information on the number of acidic residues and control of the number of ionized acidic and basic residues. *J. Am. Soc. Mass Spectrom.*, **16**, 1325–1341.

**54** Di Marco, V.B. and Bombi, G.G. (2006) Electrospray mass spectrometry (ESI-MS) in the study of metal-ligand solution equilibria. *Mass Spectrom. Rev.*, **25**, 347–379.

**55** Daniel, J.M., Friess, S.D., Rajagopalan, S., Wend, S., and Zenobi, R. (2002) Quantitative determination of noncovalent binding interactions using soft ionization mass spectrometry. *Int. J. Mass Spectrom.*, **216**, 1–27.

**56** Wortman, A., Kistler-Momotova, A., Zenobi, R., Heine, M.C., Wilhelm, D., and Pratsinis, S.E. (2007) Shrinking droplets in electrospray ionization and their influence on chemical equilibria. *J. Am. Soc. Mass Spectrom.*, **18**, 385–393.

**57** Wang, W., Kitova, E.N., and Klassen, J.S. (2003) Bioactive recognition sites may not be energetically preferred in protein-carbohydrate complexes in the gas-phase. *J Am. Chem. Soc.*, **125**, 13630–13861.

**58** Lau, Y.K., Saluja, P.S., and Kebarle, P. (1980) The proton in dimethyl sulfoxide and acetone. Results from gas-phase ion equilibria. *J. Amer. Chem. Soc.*, 7429–7433.

**59** (a) Loo, J. (1997) Studying noncovalent protein complexes by electrospray ionization mass spectrometry. *Mass Spectrom. Rev.*, **16**, 1–23; (b) Beck, J.L., Colgrave, M.L., Ralph, S.F., and Sheill, M.M. (2001) Electrospray ionization mass spectrometry of oligonucleotide complexes with drugs, metals and proteins. *Mass Spectrom. Rev.*, **20**, 61–87; (c) Daniel, J.M., McCombie, G., Wend, S., and Zenobi, R. (2003) Mass spectrometric determination of association constants of adenylate kinase with two noncovalent inhibitors. *J. Am. Soc. Mass Spectrom.*, **14**, 442–448; (d) Sun, J., Kitova, E.N., Wang, W., and Klassen, J.S. (2006) Method for distinguishing specific from nonspecific protein-ligand complexes in nanoelectrospray ionization mass spectrometry. *Anal. Chem.*, **78**, 3010–3018.